Department of Mechanical Engineering

MECH 498: Honours Thesis

Summer 2024

University of Victoria

Mass Spectrometer Superconducting Magnet Design:

Final Report

Isabel Dinneny - V00163285

Supervisor: Dr. Andrew Rowe

August 15, 2024

Abstract

The goal of this project is to design a superconducting coil that can be used in a mass spectrometer, addressing the challenges associated with resistive coils including high power consumption, large size, and field instabilities. The objectives of this project are to select a superconducting material, design and model the coil and surrounding iron, perform magnetic field and force simulations, and establish a preliminary cryogenic design.

After evaluating several materials, Rare Earth Barium Copper Oxide (REBCO) was selected. This is due to its availability and its strong critical parameters. Next, the coil was designed at an operating current of 100 A and a temperature of 65 K. After the coil cross-section was determined, the iron was designed. The iron is designed to absorb the excess magnetic field resulting from the coils. The simulations performed validated the design, confirming a uniform magnetic field of just under 1.5 T and a lack of saturation in the iron. Additionally, force simulations revealed a vertical force of 37 kN acting on each coil. The final phase of this project was establishing a preliminary cryogenic design. This included the required configuration for the vacuum chambers, thermal shields, and cryocoolers.

Looking forward, the areas for future work include developing the cryogenic system, conducting a full thermal and structural analysis, and designing the current lead.

Contents

List of Figures

List of Tables

Chapter 1

Introduction

Mass spectrometers are instruments used to measure the mass-to-charge ratios of ions and identify the compounds within a sample. Mass spectrometers function by using a magnetic field that deflects and separates ions based on their mass-to-charge ratio.

D-Pace, a company that specializes in products related to particle acceleration, produces mass spectrometers. Currently, to produce the magnetic field used to deflect the ions, D-Pace uses resistive electromagnets. As an alternative to conventional resistive magnets, D-Pace has proposed the usage of superconducting magnets. These magnets are capable of producing stronger magnetic fields while reducing power consumption. However, since superconducting properties only arise below certain temperatures, a cryogenic cooling system will need to accompany any superconducting magnets.

This project will focus on the design of a superconducting magnet for usage in D-Pace's mass spectrometer. This includes an analysis of different superconducting materials, coil and iron design, magnetic field and force simulations, and a preliminary cryogenic design.

1.1 Mass Spectrometry Background

The following section outlines the critical background information for understanding the motivation and application of this project. This includes background information on the function of mass spectrometers and the primary challenges associated with the usage of resistive magnets in mass spectrometers.

1.1.1 Function

Mass spectrometry is a tool used to measure the mass-to-charge ratio of ions. This is primarily used to determine the composition of a sample. Mass spectrometry typically consists of four main steps [1]:

- **Ionization:**

  The particles in the sample are targeted by a high-energy electron beam. This causes collisions that remove electrons from the particles. This results in positive ions.

- **Acceleration:**

  The ions are then accelerated by an electric field until they have the desired kinetic energy. This is done with a high electric potential after the ion source.

- **Deflection:**

  Upon entering the magnetic field, the ions are deflected according to their mass-to-charge ratio. Therefore, the heavier ions are deflected less and the lighter ions are deflected more.

- **Detection:**

  The final stage of mass spectrometry is ion detection. This occurs when the ion stream makes it to the detector. The detector collects the ions, converting their kinetic energy into a signal.

The processes of ionization, acceleration, deflection, and detection are shown in Figure 1.1.

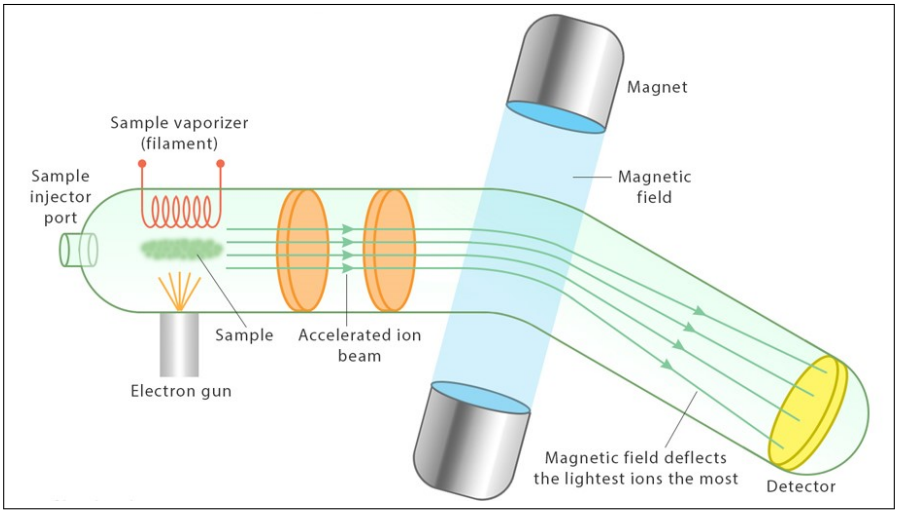

Figure 1.1: Mass spectrometer [1]

After ionization, acceleration, deflection, and detection have been completed, the ions are separated and the composition of the sample can be determined based on their mass-to-charge ratios.

1.1.2 Resistive Magnet Challenges

There are certain challenges associated with resistive magnets that could be mitigated through the usage of superconducting magnets.

- **High power consumption:**

  The conventional resistive magnets currently used in mass spectrometers dissipate energy due to resistance in the coil. This leads to increased power consumption. This resistance also leads to heat generation and in some cases, cooling systems are required to prevent component damage.

- **Increased size:**

  Resistive magnet mass spectrometers typically have a magnetic field density of 1 T. To maintain the same $B \cdot L_{eff}$ (with B being magnetic field density and L_{eff} being effective length) value, a 1 T coil requires a larger effective length. In this case, a 1.5 T coil is used, thus a smaller effective length is required. This limits the size of the assembly.

- **Field instability:**

  As resistive magnets require the constant use of a power supply, the magnetic field produced by these magnets is impacted by current fluctuations. Fluctuations in current cause field instabilities [2].

1.2 Project Objectives

This project is focused on the design and analysis of superconducting magnets to be used in mass spectrometers as an alternative to the resistive magnets currently being used. The key objectives include:

- **Superconducting material selection:**

  This project aims to select a superconducting material to use in this application. Low-temperature and high-temperature superconductors will be considered.

- **Model coils and iron:**

  Coil and iron calculations will be performed to determine the required geometry for each component. These components will then be modeled in Solidworks.

- **Simulate magnetic field and force:**

  Through the use of Ansys simulations, the magnetic field density will be determined over the span of the assembly. Additionally, the magnetic force acting on the coils will be evaluated.

- **Preliminary cryogenic design:**

  To bring the magnet to a superconducting state, it needs to be brought to cryogenic temperatures. This project aims to establish a preliminary design for the cryogenic system, including the placement of a vacuum chamber, thermal shield, and cryocooler.

1.3 Superconductivity Background

The following section discusses the properties of superconducting materials and some of the applications where they are used.

1.3.1 Superconductivity Properties

Due to the unique properties discussed in this section, superconductors offer several significant advantages for numerous potential applications.

One of the main distinguishing properties of superconductors is their ability to conduct current without any losses to resistance. This leads to the occurrence of high magnetic fields without any steady-state power consumption. For there to be no electrical resistance, the electrons in the material form Cooper pairs [3]. These pairs move through the lattice of the material without collisions or lattice vibrations (the main sources of resistance in materials). The lack of resistance enables the superconductor to carry high currents without creating excessive heat. The high current density results in stronger magnetic fields. Thus, having no electrical resistance is especially beneficial for high-field applications like nuclear fusion. Additionally, as there is no resistance, a persistent current is created. Superconductors are capable of maintaining current indefinitely without a power source. This creates stable, long-lasting magnetic fields.

Superconductors are characterized by a few critical parameters that define the conditions

under which the material is superconducting. Beyond these critical parameters, the material becomes resistive. The critical parameters are temperature, magnetic field, and current density (T_c, B_c, and J_c, respectively). These properties are related to each other in a three-dimensional space. Thus, superconducting materials are characterized by a critical surface. An example of a critical surface is shown in Figure 1.2. Below the surface of this plot, the material is superconducting but above the surface, the material is resistive [4].

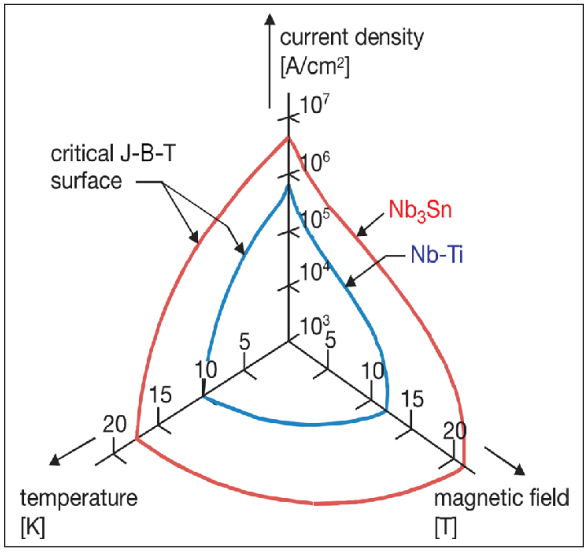

Figure 1.2: Critical surfaces example [5]

Another aspect of superconductors that dictates the properties they display is pinning centers. Pinning centers are imperfections within the material that pin magnetic vortices [6]. Vortex movement creates resistance. Thus, by introducing pinning centers (both naturally occurring and artificial), higher current densities are required to move the vortices. Therefore, with more pinning centers, the critical current density increases.

1.3.2 Applications of Superconducting Magnets

As a result of the favorable properties of superconducting materials, they are used in various applications, including magnetic resonance imaging (MRI) and nuclear fusion reactors.

- **Magnetic resonance imaging (MRI)**

  Magnetic resonance imaging (MRI), a type of non-invasive medical imaging, is one of the largest commercial applications of superconducting magnets. To date, almost 50,000 MRI machines are installed worldwide, with roughly 35,000 of them utilizing superconducting magnets [7]. These machines produce magnetic fields of primarily 1.5

T or 3 T [7]. The material typically used for superconducting MRI machines is NbTi. The MRI industry uses roughly 4000 tons of NbTi conductor per year [7]. The usage of this material necessitates the use of helium to cool the magnet to its superconducting state. Thus, the MRI industry is also one of the largest helium consumers.

A cross-sectional view of an MRI machine is shown in Figure 1.3.

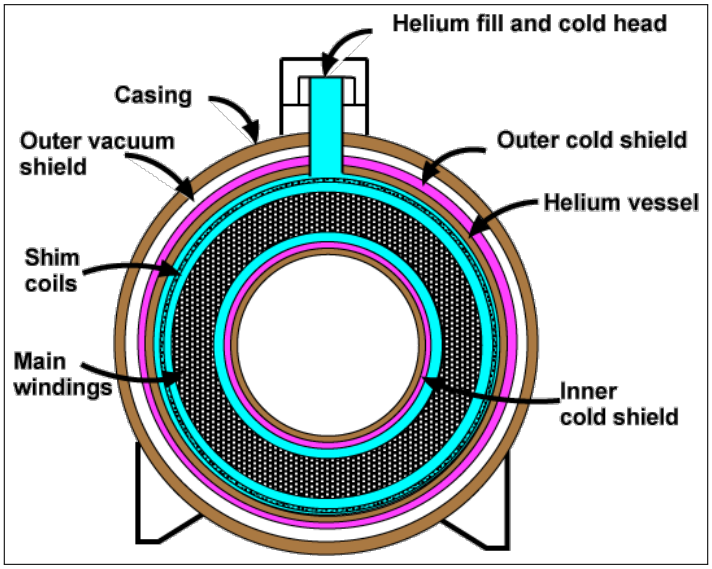

Figure 1.3: MRI machine cross section [8]

- **Nuclear fusion reactors**

  In order to achieve plasma confinement, tokamaks and stellarators (two types of nuclear fusion reactors) utilize magnetic fields. In order to reach the high magnetic fields required, many projects, both public and private, are using superconducting magnets. For nuclear fusion reactors to reach what is known as the Lawson criterion, the plasma temperature, density, and confinement time are to be maximized. Thus, superconducting magnets are used to maximize the plasma confinement time.

  ITER, the most ambitious nuclear fusion project to date, is a tokamak being built in southern France. This project is a collaboration between numerous countries. The toroidal field system requires a maximum magnetic field of 11.8 T while the poloidal field system requires a maximum magnetic field of 6 T [9]. Thus, a combination of Nb_3Sn and NbTi wires are used to produce the desired magnetic field [9].

  An image of ITER's toroidal field system is shown in Figure 1.4.

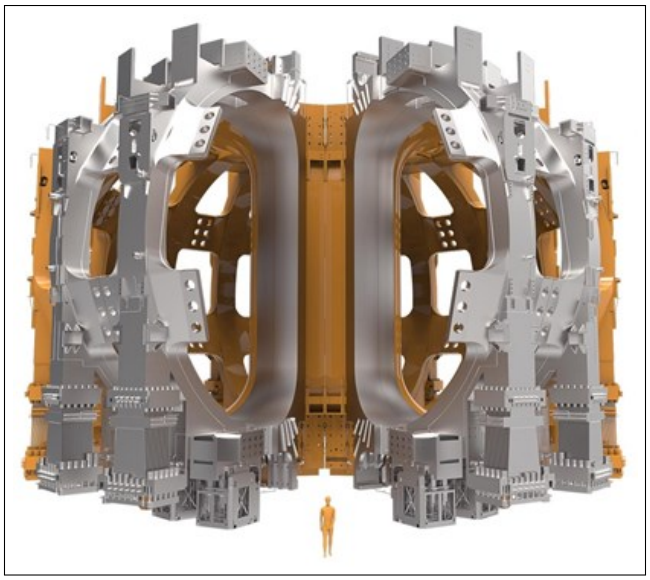

Figure 1.4: ITER toroidal field coils [9]

1.4 Summary

This chapter included background information on mass spectrometry, the objectives of the project, background information on superconductivity, and the applications of superconducting magnets. Mass spectrometers function in a four-step process of ionization, acceleration, deflection, and detection. Magnets are used to deflect the ions according to their mass-to-charge ratios. Currently, resistive magnets are primarily used for this application. Some challenges associated with resistive magnets are increased power consumption, size, and field instability. This project aims to explore the possibility of using superconducting magnets to replace resistive magnets. The scope of this project includes the selection of a superconducting material, modelling and simulating the coils to analyze the magnetic field and force produced, and designing a preliminary cryogenic system. The main distinguishing advantage of superconductors is their ability to conduct current without any losses to resistance. This creates the opportunity to produce high magnetic fields without any steady-state power consumption. As a result of this, superconductors are used for a number of applications, including MRI machines and nuclear fusion reactors.

Chapter 2

Theory

This project is heavily reliant on topics that have been established theoretically. This chapter covers the necessary theoretical background of magnetostatics and coil design.

2.1 Magnetostatics

When current does not vary with time, it is a magnetostatic system. Magnetostatic systems are governed by Maxwell's equations:

$$\nabla \cdot \vec{B} = 0 \tag{2.1}$$

$$\nabla \times \vec{H} = \vec{J} \tag{2.2}$$

where B is the magnetic flux density, H is the magnetic field intensity, and J is the current density. B and H are related by the magnetic permeability μ:

$$B = \mu H \tag{2.3}$$

For most dielectrics and metals (aside from ferromagnetic materials), $\mu = \mu_0 = 1.2566 \times 10^{-6}$ H/m.

The magnetic force F_m that acts on a charged test particle moving with velocity u through a point with magnetic flux density B is determined using the formula below. The force exerted is perpendicular to the direction of both B and u (by cross-product definition).

$$\vec{F_m} = q\vec{u} \times \vec{B} \tag{2.4}$$

Since the current flowing through a wire is made of charged particles, when a current-carrying wire experiences a magnetic field, the wire experiences a force equal to the sum of the magnetic forces acting on the particles within it. Thus, the magnetic force exerted on a charge-carrying wire is:

$$\vec{F_m} = I\vec{l} \times \vec{B} \tag{2.5}$$

where $\vec{l}$ is the vector from the current start point to the current endpoint. Thus, for a closed loop, $\vec{l} = 0$ and thus $F_m = 0$.

Currents induce magnetic fields that form closed loops around the wire. The magnetic field produced is defined by the Biot-Savart law:

$$B = \frac{\mu_0 I}{4\pi} \int \frac{d\vec{s} \times \hat{r}}{r^2} \tag{2.6}$$

where r is the distance between the current element and the point of interest.

2.2 Coil Turns

Specific to this situation, the maximum required magnetic field in the gap between poles is defined in the following way:

$$B_{max} = \frac{(33356)p}{\rho q} \tag{2.7}$$

where p is the particle momentum, ρ is the radius of curvature of the central trajectory, and q is the particle charge.

The particle momentum as it travels through the mass spectrometer channel can be calculated using the following formula:

$$p = T\Big[\frac{1}{c^2} + 2\frac{M}{T}\Big]^{1/2} \tag{2.8}$$

where p is the momentum, T is the particle kinetic energy, and M is the particle mass.

And, with the effective length, L_{eff}, and the bend angle, θ, the radius of curvature of the central trajectory, ρ, is determined:

$$\rho = \frac{L_{eff}}{\theta} \tag{2.9}$$

With the value of B_{max}, the number of trial ampere-turns per pole, NI, is calculated with an estimated 6% leakage flux and a pole gap, d.

$$NI = \frac{(0.5)(1.06)(B_{max})(d)}{\mu_0} \tag{2.10}$$

2.3 Summary

The theory related to magnetostatics and coil design was outlined in this chapter. Magnetostatics, the study of time-independent magnetic fields, is governed by Maxwell's equations (equations 2.1 and 2.2). The resulting magnetic forces on charged particles as well as on charge-carrying wires were then determined. Additionally, the Biot-Savart law was presented. This provides the magnitude of the magnetic field in a particular region. Next, the theory surrounding the maximum magnetic field in the pole gap and the number of trial ampere turns were outlined. These are the necessary equations for determining the momentum of charged particles and the geometry of the coils and notches.

Chapter 3

Literature Review

This literature review includes an overview of superconducting materials, including their manufacturing and fabrication methods as well as their critical parameters. Additionally, the process of coil design is explored, including an overview of superconducting materials and several studies that have utilized superconducting magnets for comparable applications.

3.1 Superconducting Material Properties

Since the discovery of superconductivity in 1911 by Heike Onnes, significant research has been conducted into superconducting materials. These materials are currently in different stages of development, with some being fully commercialized while others have not yet developed past laboratory research.

A plot of superconducting materials and their critical parameters is shown in Figure 3.1.

The following section discusses three superconducting materials: NbTi, REBCO, and BSCCO.

3.1.1 Niobium-Titanium (NbTi)

Niobium titanium (NbTi), a low-temperature superconducting material, is currently one of the most widely used superconducting materials. This is due to its ductility (thus easier manufacturing) and relatively cheap raw materials. NbTi wires are manufactured by casting an alloy into ingots, melting the ingots into rods which are inserted into copper tubes. These are heated and extruded repeatedly until it is drawn to their final size [11]. A cross-section of this wire is shown in Figure 3.2.

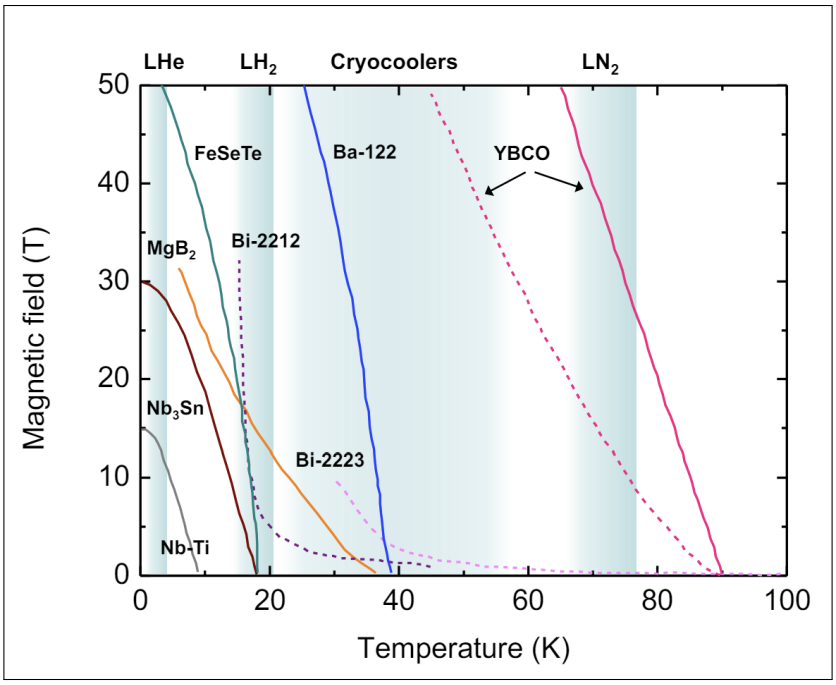

Figure 3.1: B-T plot [10]

NbTi is typically utilized in intermediate magnetic fields[11]. NbTi has a maximum critical temperature of 9.5 K with a critical current density of 4×10^5 A/cm^2 [10].

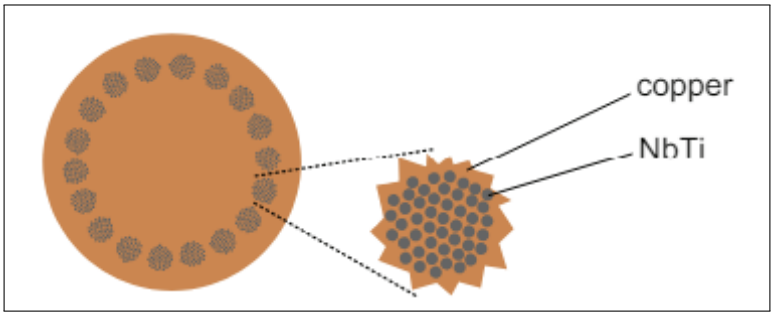

Figure 3.2: NbTi wire cross section [11]

3.1.2 Rare Earth Barium Copper Oxide (REBCO)

Rare Earth Barium Copper Oxide (REBCO) is a high-temperature superconductor that can be used in a wide number of applications. REBCO tape is manufactured through a series of thin film deposition processes. The layers are shown in Figure 3.3. REBCO utilizes high-strength alloy substrates, including Hastelloy C-276 or stainless steel [12]. The REBCO layer itself is fabricated using either chemical deposition techniques or physical vapor deposition techniques[12].

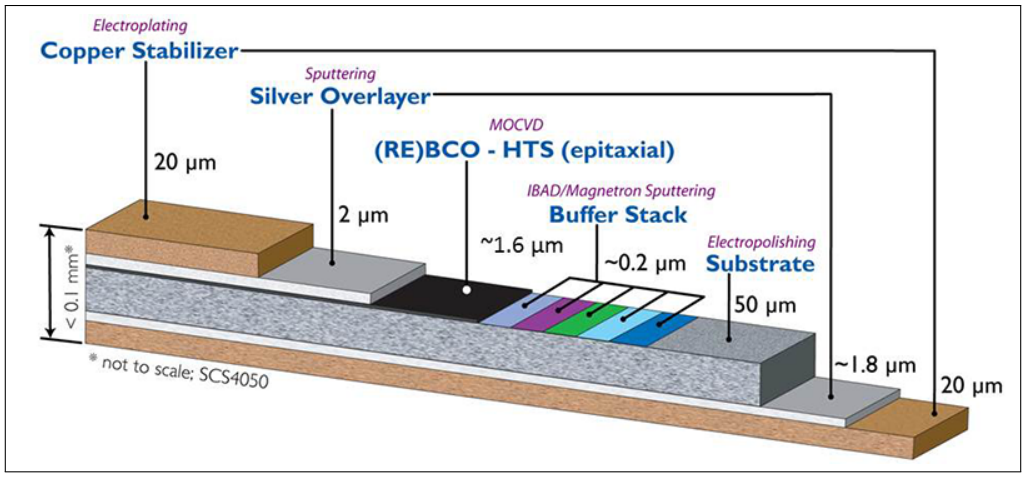

Figure 3.3: REBCO tape layers [13]

REBCO can be used for high or low-field applications. At the maximum critical temperature, T_c of 92 K, a low magnetic field can be obtained (less than 3 T) [10]. REBCO also has a critical current density of 10^7 A/cm^2, one of the highest critical current densities of all superconductors at 4.2 K.

3.1.3 Bismuth Strontium Calcium Copper Oxide (BSCCO)

Bismuth Strontium Calcium Copper Oxide (BSCCO) is another high-temperature superconducting material. BSCCO comes in a number of different compositions. The most common types of BSCCO are BSCCO-2212 and BSCCO-2223. As shown in Figure 3.1, BSCCO-2223 has a higher critical temperature for low magnetic field applications and it also has a higher current density [10]. BSCCO-2223 has a maximum critical temperature of 108 K [10].

BSCCO-2223 tapes are typically manufactured using a powder-in-tube process. The raw materials are milled, sintered and then used to fill tubes. The tubes are extruded and then a bundle of tubes is formed. These are again extruded. After cycling through several times, heat treatment occurs in an oxygen rich environment in order for oxidation to take place [11]. Due to chemical compatibility and oxygen permeability, silver is used in the tubes [10].

A cross-section of BSCCO tape is shown in Figure 3.4.

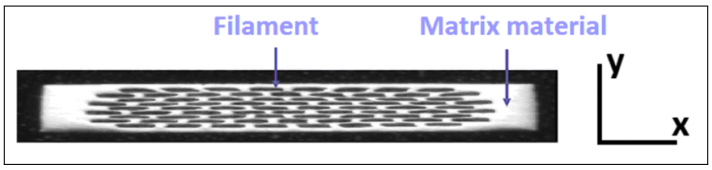

Figure 3.4: BSCCO tape cross section [14]

3.2 Coil Design

Three cases of coil design will be explored in this section.

Cryogen free 1.5 T YBCO magnet for MRI [15]

A cryogen-free 1.5 T magnet made of YBCO (high-temperature superconductor) was designed to be used in MRI machines. The motivation behind this project was the rising cost of liquid helium which would typically be used to cool low-temperature superconductors.

This design utilizes 16 pancakes made from a total of 4.8 km of YBCO conductor (produced by AMSC). The magnet operates at 20 K and 130 A. The performance of the conductor was measured at different temperatures and field angles due to the anisotropy of YBCO. The forces on the coils were calculated using OPERA. The structure uses G-10 axial struts and stainless steel tension elements to provide structural support and minimize thermal conductivity. Figure 3.5 shows the temperature distribution through the assembly. A Cryomech PT-810 pulse tube cryocooler is used for cooling. Cooling to the required 20 K took approximately 40 hours.

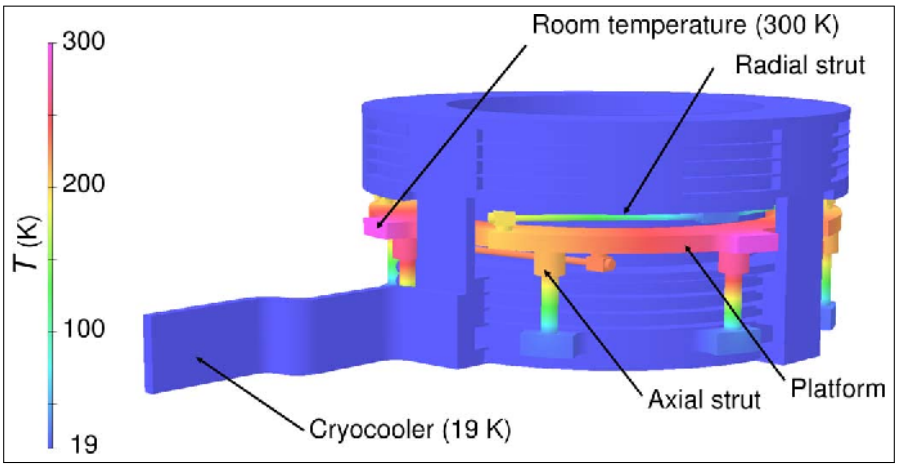

Figure 3.5: Temperature distribution through magnet coil and suspension elements [15]

Design of a superconducting 32 T magnet with REBCO high field coils [16]

The design and fabrication of a 32 T superconducting magnet with REBCO inner coils was undertaken at the National High Magnetic Field Laboratory (NHMFL). This project aimed to demonstrate technical advancement while balancing cost and risk (thus, a 32 T field).

The magnet includes a 15 T low-temperature superconducting background coil and a 17 T REBCO inner coil. One of the main aspects of design explored was the winding insulation. Insulation thin enough for the high current density windings was not provided by the supplier.

The insulation selected combines insulated stainless steel with sol-gel ceramics. This provides effective thermal conductivity while reducing thickness.

Another design aspect was the quench protection. To address the issue of quenching, distributed heaters were incorporated. Independent power supplies and quench detectors would be activated during a quenching event.

The coils were eventually fabricated and tested successfully. A cross-section of the 32 T magnet is shown in Figure 3.6.

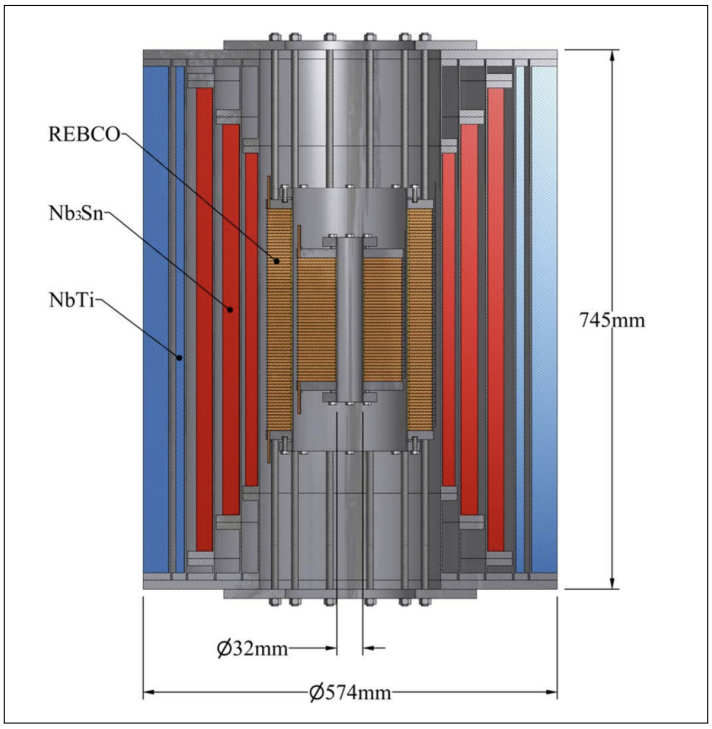

Figure 3.6: Cross section [16]

A compact 3 T all HTS cryogen-free MRI system [17]

This project is on the design and fabrication of a compact 3 T high-temperature superconductor for a cryogen-free MRI system. This MRI machine is primarily designed for small animal imaging. This project uses BSCCO (as opposed to REBCO). This magnet was cooled to 16 K using a two-stage Gifford-McMahon cryocooler and then operated at a current of 200 A. The magnet uses 18 double pancake coils made from BSCCO tape and contained in epoxy resin. The magnet design includes a two-layer steel yoke that is used for magnetic shielding. Additionally, quench protection was introduced.

After design and fabrication, it was found that the magnet achieves the desired 3 T field strength.

An image of this assembly is shown in Figure 3.7.

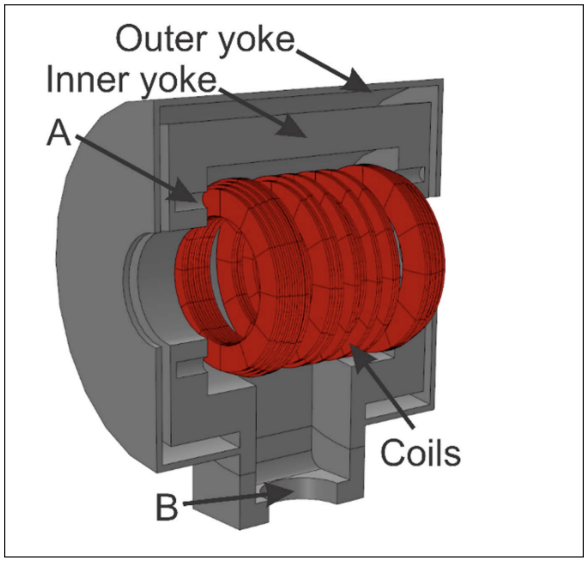

Figure 3.7: Cross section of magnetic assembly. Label A shows feature for axial suspension of coil pack. Label B shows the entry point for the cryocooler. [17]

3.3 Summary

The literature review conducted includes two main areas of interest: the properties of superconducting materials, and cases of coil design. The properties of three different materials were studied. These materials include niobium titanium (NbTi), rare earth barium copper oxide (REBCO), and bismuth strontium calcium copper oxide (BSCCO). NbTi is a low-temperature superconductor that is relatively simple to manufacture due to the ductility of the material. REBCO is a high-temperature superconductor that has become more prevalent in recent years. It is manufactured through a series of thin film deposition processes. BSCCO is also a high-temperature superconductor. It is manufactured using a powder-in-tube process. The matrix in the tubes is silver due to its chemical compatibility and oxygen permeability. The coil design cases explored include a cryogen-free 1.5 T REBCO magnet for an MRI machine, a high field apparatus using REBCO coils, and a 3 T BSCCO MRI system. These studies outlined the thermal, structural, and magnetic field setups for each of the cases.

Chapter 4

Methods

This chapter outlines the methods utilized in the design of the superconducting coils. The scope of design and analysis included in this project includes designing the coil in terms of material and geometry, designing the outer iron that absorbs the stray magnetic field, performing magnetic field simulations to verify field uniformity and iron saturation, performing force simulations to determine the required structural components to support the coils, and designing a preliminary cryogenic system.

4.1 Material Selection

The superconducting coil material is selected using a weighted decision matrix. In this method, a list of factors is weighted and then each of the materials is scored using these weights. This is a quantitative method to assess materials.

The weighted decision matrix takes the following factors into account:

- **Critical temperature:** higher critical temperatures allow for reduced cooling requirements and simpler, less power-intensive cryogenic systems.
- **Critical current:** higher critical currents allow for more current to flow through the superconducting material and thus a smaller cross-sectional coil area.
- **Availability:** with superconducting materials emerging in recent years, it is important to evaluate the level of commercialization and overall material availability.
- **Cost:** as this is for a commercial application, the cost of the material is an important consideration. The cost is a function of the cost of raw materials and the ease of

fabrication.

The weights of each of these factors is shown in Figure 4.1.

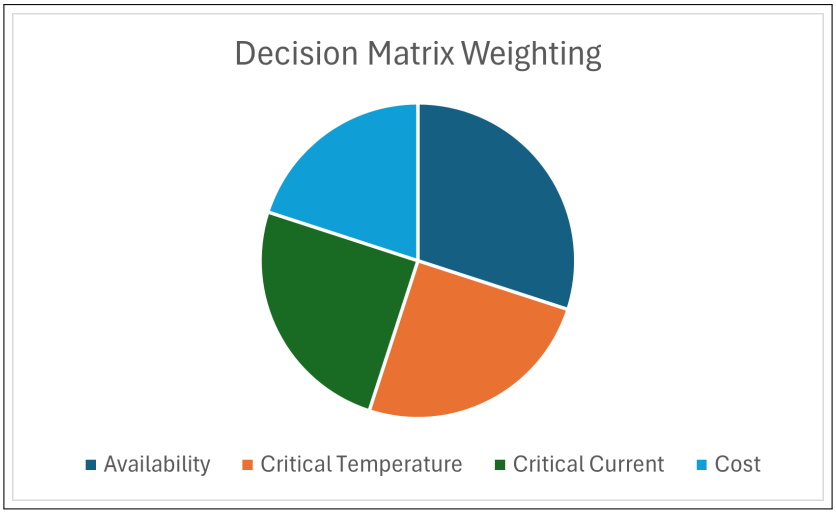

Figure 4.1: Decision matrix weighting

4.2 Initial Specifications

There are several specifications that the design is to adhere to. These quantitative specifications are used in the design of the coil and iron. The specifications are outlined in Table 4.1.

Table 4.1: Initial specifications

Specifications	
Magnetic field in gap	1.518 T
Bend angle	125 deg
Effective length	675 mm
Pole face angle	48.9289°
Pole gap	100 mm
Bend direction	Right
Drift distance entrance	400 mm
Drift distance exit	400 mm
Ion mass	Up to 176 AMU
Ion charge state	+1
Maximum kinetic energy	60 keV
Particle momentum	140.26 MeV/c
Central trajectory radius of curvature	309.4 mm
Number of trial ampere-turns per pole	64 023 Amp Turns

4.3 Coil and Iron Design

The following calculations are required to determine the coil geometry and the notch geometry. Additionally, this section includes power consumption calculations for a resistive magnet.

Coil Geometry

Using the calculated values for mass and momentum (Equation 2.8), along with the radius of curvature of the central trajectory (Equation 2.9), the maximum magnetic field in the pole gap, B_{max}, is determined (Equation 2.7). Then, using this value, the number of trial ampere-turns per pole, NI is found.

Using a maximum current for the specified material, the number of turns per coil can be determined:

$$N_{turns} = \frac{NI}{I_{max}} \tag{4.1}$$

Consider a strip wound coil utilizing superconducting tape and Mylar insulation. There is a certain number of pancakes per coil with a top, middle-upper, middle-lower, and bottom aluminum cooling plates each with a fiberglass pancake wrap (Half-Lapped technique, minimum 2 layers) and a fiberglass overwrap on all sides (Half-Lapped technique, minimum 8 layers).

Therefore, the current density in the magnet is:

$$J_{max} = \frac{I_{max}}{ht} \tag{4.2}$$

where t and h are the thickness of the selected tape.

At this point, the coil width can be determined.

$$\text{Coil width= (Conducting tape) + (Mylar) + (Pancake wrap) + (Coil over-wrap)} \tag{4.3}$$

Next, the coil height can be determined.

$$\text{Coil height= (Mylar) + (Cooling plate) + (Pancake wrap) + (Coil over-wrap)} \tag{4.4}$$

Notch Geometry

A good field region is defined on either side of the central trajectory in the horizontal and

vertical bend planes. A D-Pace rule of thumb is that a pole width that is a factor of 5 times as large as the good field region will achieve the desired level of uniformity.

As a result of this rule of thumb, the pole width w is equal to:

$$w = (5)(f) \tag{4.5}$$

where f is the defined field width.

In the resistive coil case, the coil notch in the yoke is chosen to be the coil width plus 5 mm buffer space on either side of the coil to ensure there is enough space for the epoxy-potted coil to fit in the magnet. The notch height for the coil (up to the top of the pole chamfer of 10 mm) is coil height plus 3 mm to include space for neoprene underneath the coil.

Using the previously defined coil width and height, the notch width and height are determined:

$$\text{Coil notch width} = w_{coil} + (2)(5\,\text{mm}) \tag{4.6}$$

$$\text{Coil notch height} = h_{coil} + 3\,\text{mm} \tag{4.7}$$

Next, the yoke area is determined. To do this, the pole area needs to be determined.

The radius of curvature ρ was defined above. Additionally, the pole width was determined to be $5f$.

The partial pole (P1) width is half of the pole width. The outer radius of P1 is therefore $\rho + 5f/2$. The partial pole (P2) width is the same as the partial pole (P1) width. The outer radius of P2 is the central trajectory. The inner radius of P2 is therefore $\rho - 5f/2$. The pole areas can then be found after modelling the poles in Solidworks.

With this information, the yoke cross-sectional areas are found. It is desired to have a larger field in the poles than in the yokes. Therefore, the yoke areas are to be larger than the pole areas by a factor of 1.5/1.2.

$$(1.2)A_{yoke} = (1.5)A_{pole} \tag{4.8}$$

Power Consumption

To determine the coil power for the resistive magnet (copper coil), electrical calculations can be performed. Coil power will be an important metric when considering the switch to a superconducting coil.

From the previously determined coil geometry, the median turn length L_{turn} is found.

Therefore, the total conductor length per coil is equal to:

$$\text{Total conductor length per coil} = (N_{turns})(L_{turn}) \tag{4.9}$$

Next, at a temperature of 20°C, the resistance can be determined.

$$R_{20^o} = \rho_{Cu}\frac{\text{Total Conductor Length}}{\text{Conductor Cross-Sectional Area}} \tag{4.10}$$

Using this value and the assumption that the maximum ΔT is 40°, the resistance R_{hot} is calculated.

$$R_{hot} = R_{20^o}[1 + (\Delta T)(\text{Temperature Coefficient of Copper}) \tag{4.11}$$

With this value, along with the current I_{max}, the voltage drop per coil is found.

$$V_{coil} = (I_{max})(R_{hot}) \tag{4.12}$$

Therefore, the power requirement for the entire magnet (2 coils) is:

$$P = (2)(V_{coil})(I_{max}) \tag{4.13}$$

4.4 Magnetic Field and Force Simulations

Ansys Maxwell is used to conduct magnetic field and force simulations for both of the coil geometries. The main purposes of these simulations are to analyze the field uniformity through the region where the particles travel, to assess the surrounding iron to determine if the material gets saturated with the magnetic field, and to evaluate the forces that are to be structurally supported.

4.4.1 Ansys Maxwell Method

Ansys Maxwell utilizes the finite element method (FEM) to numerically solve Maxwell's equations (equations 2.1 and 2.2) and the magnetic force equation (equation 2.5). The assembly geometry is divided into small, finite elements (the mesh). Within each element, the field and force are determined. Based on the magnetic field in each element, a contour plot is produced. For the force simulations, force values exerted on a body are produced.

4.4.2 Simulation Set-Up

The following sections outline the boundaries, excitations, meshes, and material properties that are to be conducted in each of the cases for simulations using Ansys Maxwell.

Boundaries

The two boundaries set in this simulation are both insulating. This boundary is applied to each of the coils in the assembly. This boundary specifies the normal component of the magnetic field to be zero at the boundary. This is done to ensure that there is no current flow crossing the boundary.

$$B_n = 0 \tag{4.14}$$

Excitations

There are current excitations through both coils in the assembly. These excitations were defined by making cross-sectional planes through the coils and applying a current excitation. The current excitation is defined by two variables: current and turns.

The allowable current depends on the temperature of the superconducting coil. Using the critical current parameters, the operating current values were obtained. Due to the possibility of temperature fluctuations during operation, current values 10 A lower than the critical values were used as operating currents.

$$I_{operating} = I_c - 10\,\mathrm{A} \tag{4.15}$$

With an estimated leakage flux, maximum magnetic flux density, and pole gap, the number of ampere-turns required can be determined according to Equation 2.10. Using this value, the number of turns per coil N_{turns} is determined:

$$N_{turns} = \frac{NI}{I_{operating}} \tag{4.16}$$

Using the option for stranded (as opposed to solid) current excitation, along with the values for $I_{operating}$ and N_{turns}, the current excitation is defined through cross-sections in each coil:

$$NI = N_{turns} \cdot I_{operating} \tag{4.17}$$

Mesh

Due to the overall simple geometry of the components in this assembly, an auto-generated mesh from Ansys was used. The mesh is shown in Figure 4.2 below. As shown in this Figure, the mesh is relatively coarse. This is due to the limit on the number of elements that can be used in the student version of Ansys.

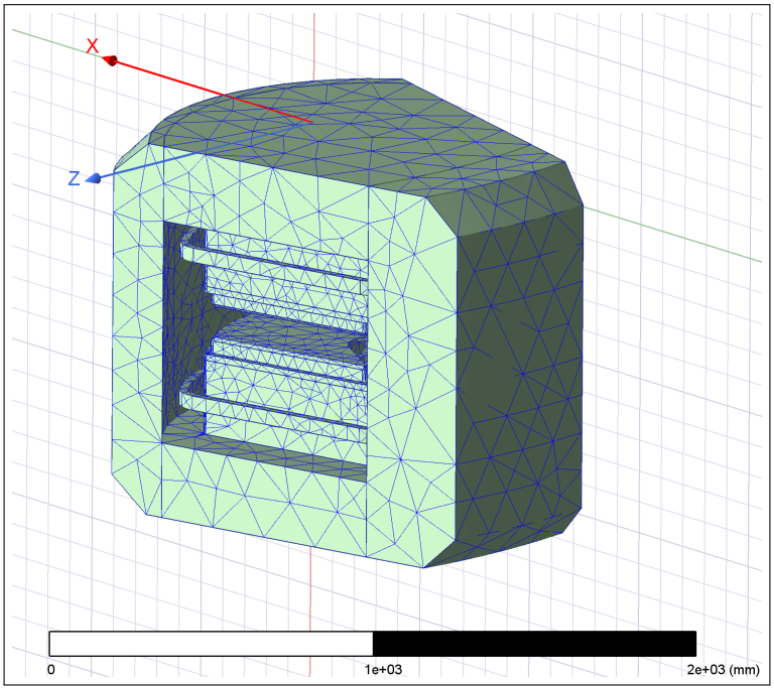

Figure 4.2: Assembly mesh

Material Properties

The materials that are to be used for this project are superconducting tape for the coils and C1006 Iron for the remainder of the components. As these materials are not available in Ansys's materials library, the material properties had to be defined.

For superconducting materials, the relative permeability should be zero. However, since Ansys does not take zero values for this field, a number approaching zero was used (1×10^{-7}). Additionally, for superconducting materials, since there is no resistance while in a superconducting state, the bulk conductivity of the tape is infinite. Since Ansys does not take infinite values, 1×10^{9} S/m was used. The remainder of the properties were set to default values. A summary of the relevant magnetism properties used is shown in Table 4.2.

C1006 Iron, iron with very low carbon content, is very similar to low carbon steels including 1006 Steel and 1008 Steel. The main differences come from minor alloying elements and

Table 4.2: Superconducting material magnetic properties

Property	Value	Units
Relative Permeability	1e-07	-
Bulk Conductivity	1e+09	S/m

impurities that slightly alter properties. However, for the purposes of this simulation, these materials can be used interchangeably. The relevant magnetic properties for this simulation are shown in Table 4.3 and in Figure 4.3.

Table 4.3: 1006 Steel magnetic properties

Property	Value	Units
Relative Permeability	B-H Curve (Fig. 4.3)	-
Bulk Conductivity	2e+06	S/m

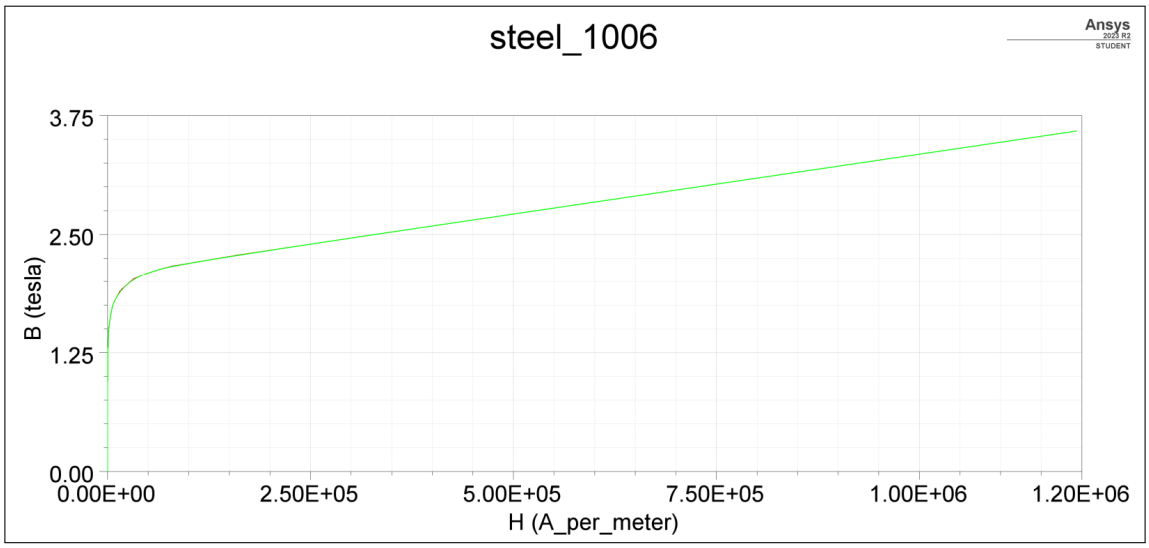

Figure 4.3: 1006 steel B-H curve

4.5 Cryogenic System

The final part of this project is to design a preliminary cryogenic system to contain and cool the superconducting coils. This design is to be created using a Solidworks model. This design includes the following key components:

- **Supports:** supports around the coils are used as the primary structural members. These are to be designed to minimize thermal conductivity while maintaining structural stability.

- **Vacuum chamber:** the vacuum chamber is designed to enclose the superconducting magnet. Additionally, it needs to be large enough to contain the thermal shield and insulation that surround the magnet.
- **Cryocooler connection:** the cryocooler connection point and cold head position are designed to feed into the vacuum chamber without compromising the performance of the iron.

4.6 Summary

This chapter outlines the methods used throughout this project. First, a series of values are obtained in order to determine the coil geometry. Then, using these values, the geometry of the iron and the overall power consumption are determined. In the next section, the methods used to set up the magnetic field and force simulations in Ansys Maxwell are discussed. This includes setting up boundary conditions, current excitations, a mesh, and the material properties. Finally, the method for approaching the preliminary cryogenic system design is discussed. This includes describing the critical components that are required.

Chapter 5

Results

The results of material selection, coil design, magnetic field simulations, magnetic force simulations, and preliminary cryogenic design are presented in this chapter. The material selection process is conducted using a weighted decision matrix. The coil design results include the geometric configurations of the coils for different cases. The magnetic field simulation results include contour plots for each of the coil configurations. The magnetic force simulation results consist of force values experienced by the coils in each direction. The preliminary cryogenic design results show initial drawings of the system.

For each of these sections, any detailed calculations performed are presented in the corresponding appendix section. Additionally, preliminary drawings are shown in Appendix D.

5.1 Material Selection

The superconducting coil material was selected using a weighted decision matrix. The weighting factors include material availability, critical temperature, critical current, and cost.

The materials compared were NbTi, REBCO, and BSCCO. Using the weighting factors, each of the materials was scored. The final weighted decision matrix is shown in Table 5.1. As shown in this Table, the scores for NbTi, REBCO, and BSCCO are 3.75, 4.3, and 3.25, respectively.

Therefore, REBCO is the selected material.

Table 5.1: Weighted decision matrix

Factor	Weight factor	NbTi		REBCO		BSCCO	
		Score	Value	Score	Value	Score	Value
Material availability	30 %	5	1.5	4	1.2	2	0.6
Critical temperature	25 %	1	0.25	5	1.25	5	1.25
Critical current	25 %	4	1	5	1.25	4	1
Cost	20 %	5	1	3	0.6	2	0.4
Total			**3.75**		**4.3**		**3.25**

5.2 Coil Design

Using the series of calculations presented in Chapter 4, the cross-sectional area for two coil configurations can be determined. The coil calculations utilize the Fujikura REBCO tape parameters. A plot showing the critical current at a given temperature and magnetic field is shown in Figure 5.1.

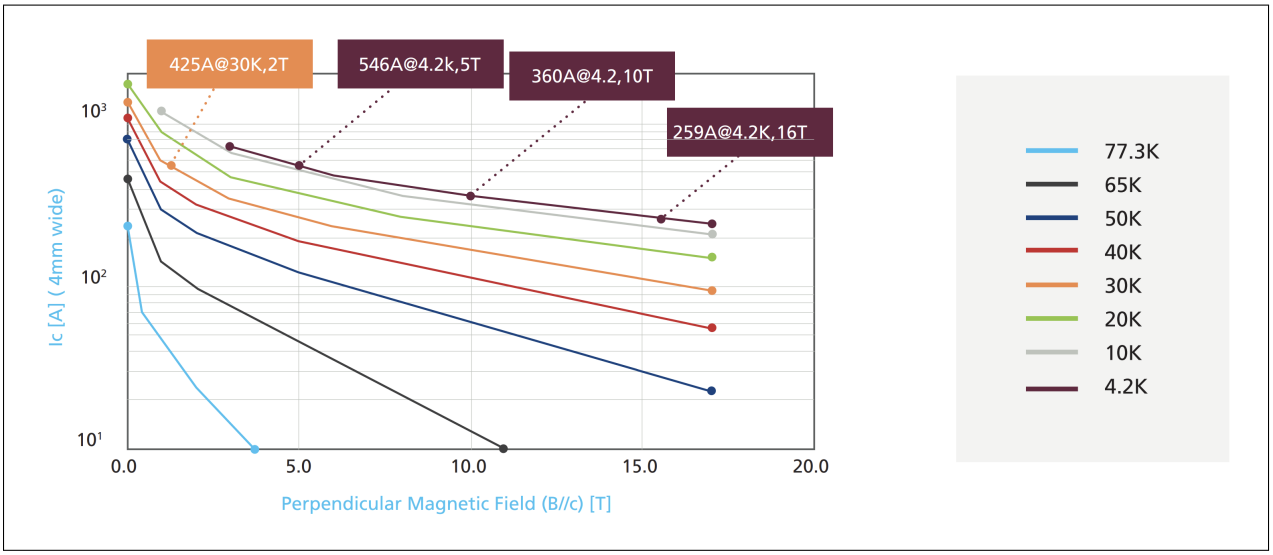

Figure 5.1: Fujikura REBCO tape parameters [18]

Two different coil cross-sections were determined with varying numbers of pancakes. The resulting cross-sectional dimensions for the two cases are shown in Table 5.2.

Table 5.2: Coil cross-section dimensions

Case	Temperature [K]	Pancakes [-]	Current [A]	Turns per coil [-]	Coil width [mm]	Coil height [mm]
1	65	3	100	641	50	46
2	65	4	100	641	39	56

A MATLAB function can be used to perform the calculations in a repeatable, error-free manner. The MATLAB code is shown in Appendix A.1.

Full sample calculations for determining the coil geometry for a resistive copper coil are shown in Appendix A.2.

An isometric view of the 3 pancake coil is shown in Figure 5.2.

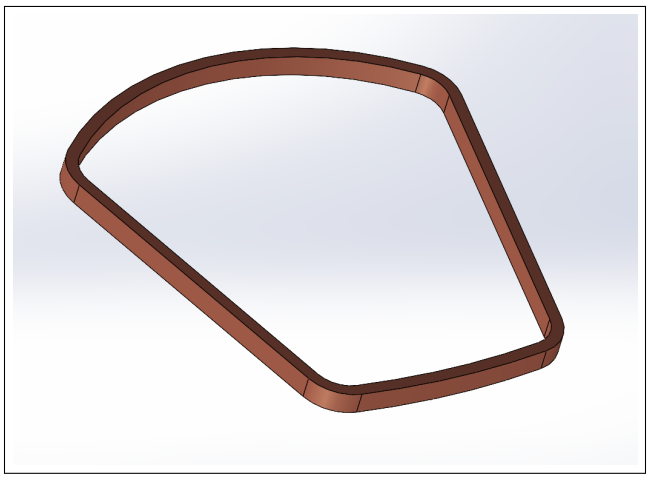

Figure 5.2: Isometric view of 3 pancake coil

5.3 Iron Design

The design of the iron (including the notch geometry) is based on the initial design of a resistive coil with a width and height of 117 mm and 297 mm, respectively. Using these values, along with the pole width, and pole face angle leads to the pole and iron geometry, as shown in Figures 5.3 and 5.4.

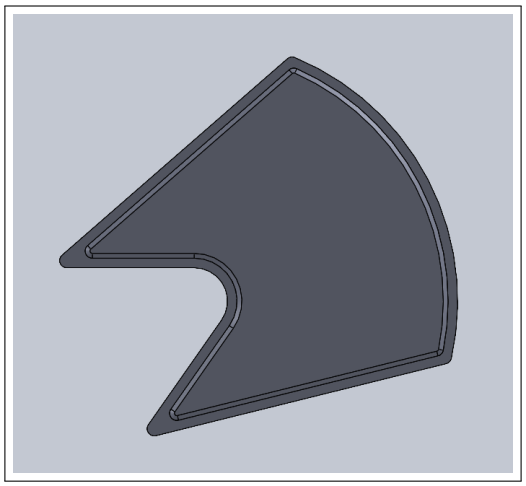

Figure 5.3: Pole geometry

Appendix B includes full calculations for the iron and pole design.

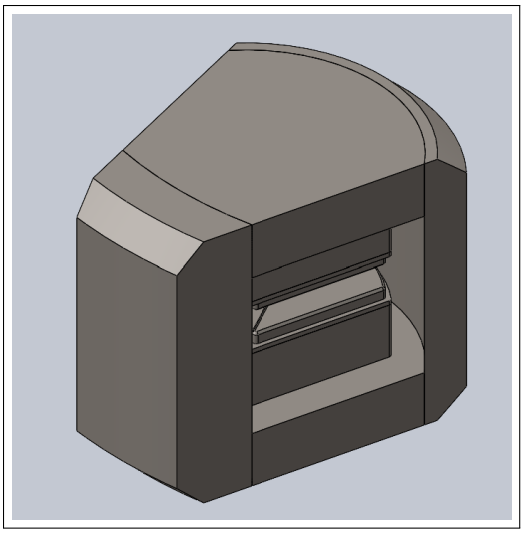

(a) Isometric view

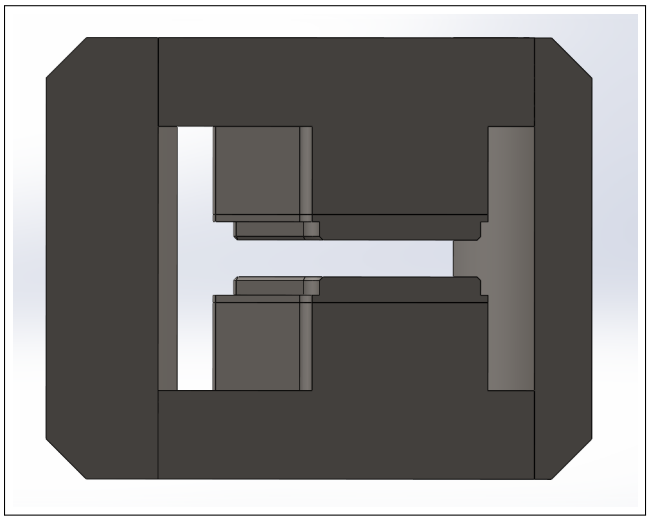

(b) Sectioned view

Figure 5.4: Iron geometry

5.4 Resistive Coil Power Consumption

The total power consumption of the resistive coil can be determined using the resistive coil geometry. With the total conductor length within a coil, the total resistance through each coil is found. This value, along with the current, leads to the voltage drop per coil. Ultimately, this results in a total power consumption of 17.3 kW.

Appendix C includes full calculations for the power consumption of a resistive magnet.

5.5 Magnetic Field Simulations

With the parameters outlined in Chapter 4.4, the magnetic field simulations for the two coil geometry cases were conducted and contour plots were obtained. Figure 5.5 and 5.6 show the contour plots for each of the coil geometries.

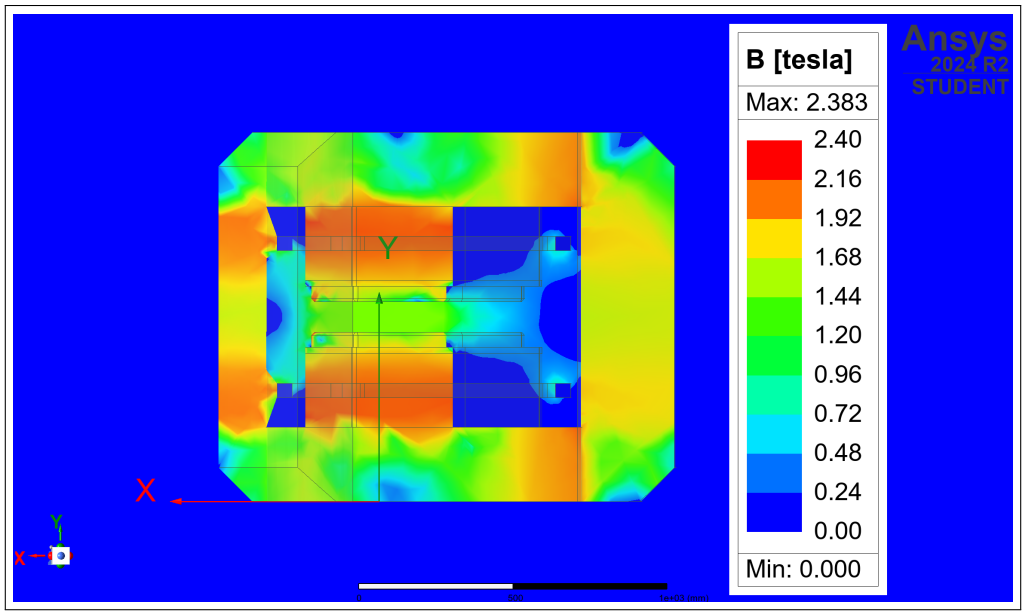

Figure 5.5: Case 1 - magnetic field contour plot (65 K, 100 A, 3 pancakes)

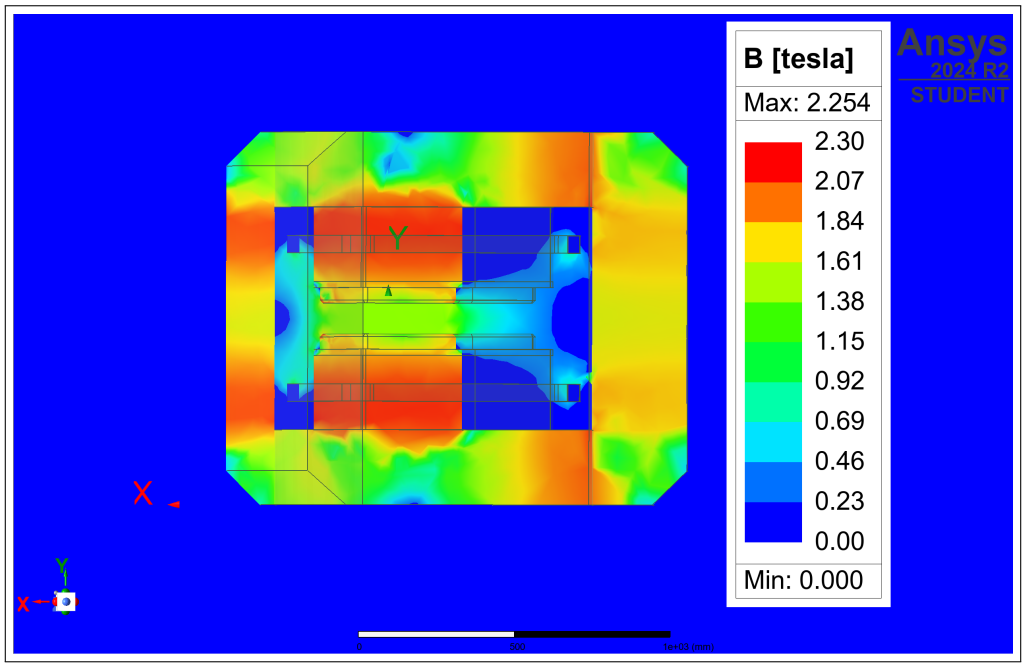

Figure 5.6: Case 2 - magnetic field contour plot (65 K, 100 A, 4 pancakes)

5.6 Magnetic Force Simulations

In Ansys Maxwell, the virtual force acting on each coil was also determined. The values in the top and bottom coils for each case are shown in Table 5.3. The force directions as well as the definitions of “Top” and “Bottom” are shown in Figure 5.7

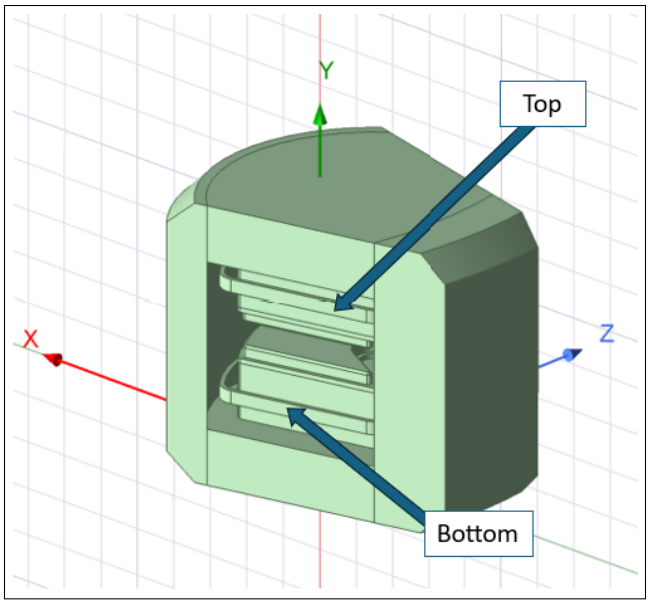

Figure 5.7: Force directions

Table 5.3: Magnetic force values

Case	Coil	F(x) [N]	F(y) [N]	F(z) [N]	|F| [N]
1	Top	732	36 333	33	36 341
	Bottom	719	-36 258	5	36 265
2	Top	292	37 383	-111	37 384
	Bottom	612	-36 380	1	36 385

5.7 Preliminary Cryogenic Design

This preliminary design of the cryogenic system includes the layout of the vacuum chamber, thermal shield, cryocooler, and structural supports. This is a preliminary concept based on minimal analysis. A cross-sectional view of this concept is shown in Figure 5.8.

5.8 Summary

This chapter goes through the results of each of the phases of this project. First, the results from the weighted decision matrix were presented, indicating that the selected material is REBCO. Next, the resulting coil and iron designs were revealed. The next phase of the project was performing simulations for the magnetic flux density and magnetic force on the coils. The magnetic flux density contour plots were presented, as well as the force data for the coils. Finally, the resulting cryogenic design was shown.

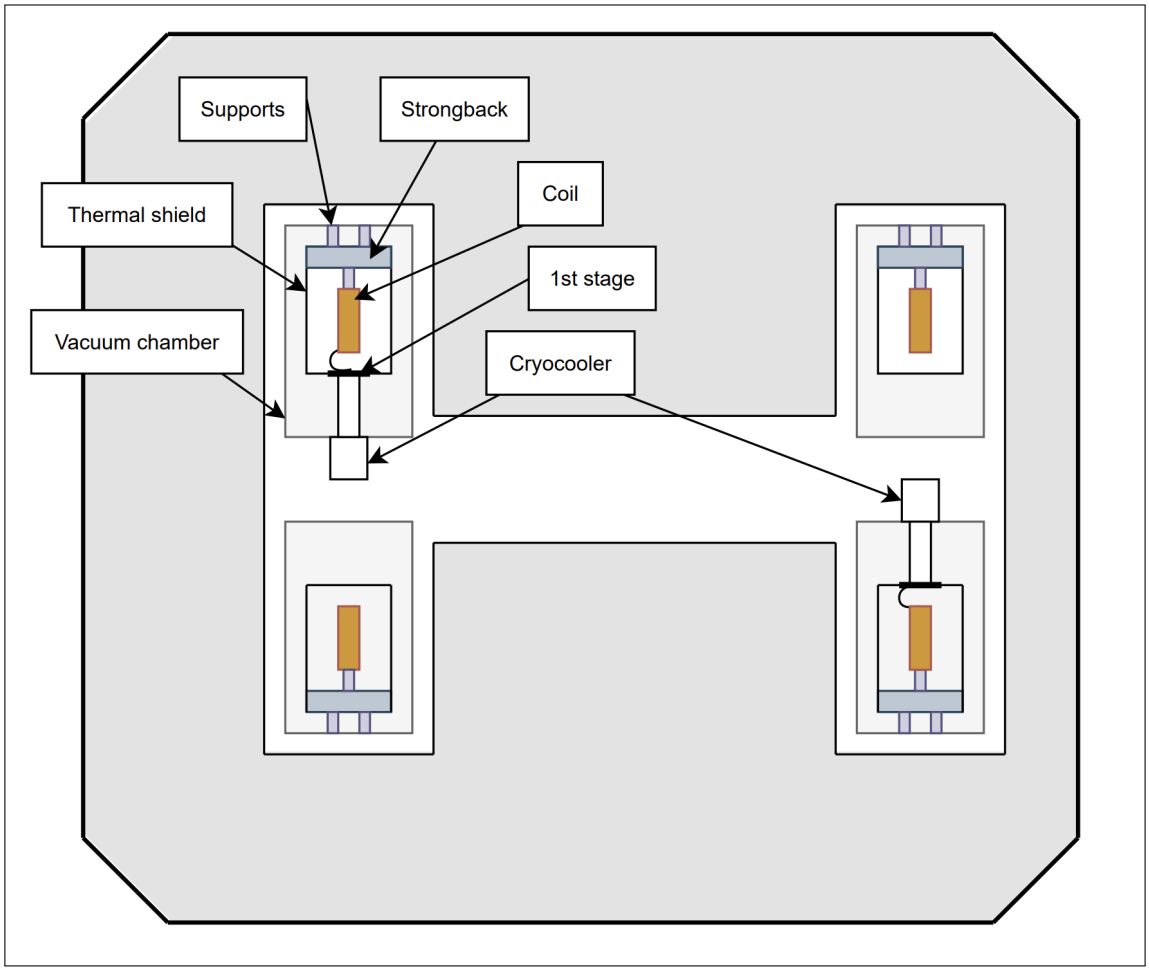

Figure 5.8: Preliminary cryogenic layout (cross-sectional view)

Chapter 6

Discussion

This chapter explores and analyzes the results presented in the previous chapter. This includes deeper insight into the superconducting material selection, the decision rationale behind the coil and iron design, conclusions drawn from the simulations, and design features of the cryogenic system.

6.1 Superconducting Material Selection

This section goes through the the rationale behind the selection criteria that was used for evaluating the superconducting materials. Additionally, further information on the selected material is presented.

6.1.1 Selection Criteria

Three superconducting materials were considered for this project: NbTi, REBCO, and BSCCO. When selecting materials for consideration, the level of commercialization and the critical temperature were important factors. NbTi is one of the most widely used superconducting materials available. REBCO and BSCCO are both promising high-temperature superconductors. The high critical temperatures of these materials allow for the usage of single-stage (lower power consumption) cryocoolers.

When narrowing down to select one final material, the weighted decision matrix in Table 5.1 was used. The weighted factors are material availability, critical temperature, critical current, and cost. These were assigned weight factors of 30%, 25%, 25%, and 20%, respectively. A pie chart of these weights is shown in Figure 4.1.

NbTi, being one of the most widely used superconducting materials, performed well in the material availability category. However, at 9.5 K, the most significant issue with NbTi is its critical temperature. Being a low-temperature superconductor, the critical temperature of this material is lower than desired. At 4.2 K, the critical current density of this material is 4×10^5 A/cm^2. This value is lower than the critical current densities of REBCO and BSCCO but is still relatively high. The final area considered was cost. NbTi scored well in this category as it is readily available and is simple to manufacture.

The next material considered is REBCO. This superconducting material is produced in tape form by several companies including SuperPower, Fujikura, Sumitomo, and Bruker (among others). As this technology continues to develop, the production is increasing. As this is a high-temperature superconductor, the maximum critical temperature is 92 K. This value, along with the critical current density on the order of 10^7 A/cm^2 leads REBCO to score highly in both the critical temperature and critical current categories. As REBCO has a complex manufacturing process and has only been developed relatively recently, REBCO tape is more expensive than some other options. However, the raw material cost for REBCO tape is low.

The final material that was evaluated was BSCCO. The main issue with this material is its availability. With the emergence of REBCO, BSCCO has become less prevalent. At present, one of the only producers of BSCCO-2223 is Sumitomo. With a maximum critical temperature of 108 K and a critical current density of 10^6 A/cm^2, the critical parameters for this material offer promise. The cost of this material, which directly results in the lack of availability, is high. As it is required to have a silver or silver alloy matrix, along with the complex manufacturing process, materials and manufacturing of BSCCO tape is expensive. The expense of this material, as well as the comparable properties to REBCO is leading to a reduction in BSCCO usage.

6.1.2 Selected Material

After using the weighted decision matrix shown in Table 5.1, REBCO is the selected material for this project. REBCO tapes consist of a series of layers deposited using thin film deposition processes. The manufacturers that make REBCO tape use relatively similar layer thicknesses and materials. Thus, the Fujikura REBCO tape properties are selected to be used for the remainder of this project. It should be noted that quotes have not been obtained and a different manufacturer could perform better for these project requirements. The layers of this tape are shown in Figure 6.1 and the critical current plot at different temperatures is

shown in Figure 6.2.

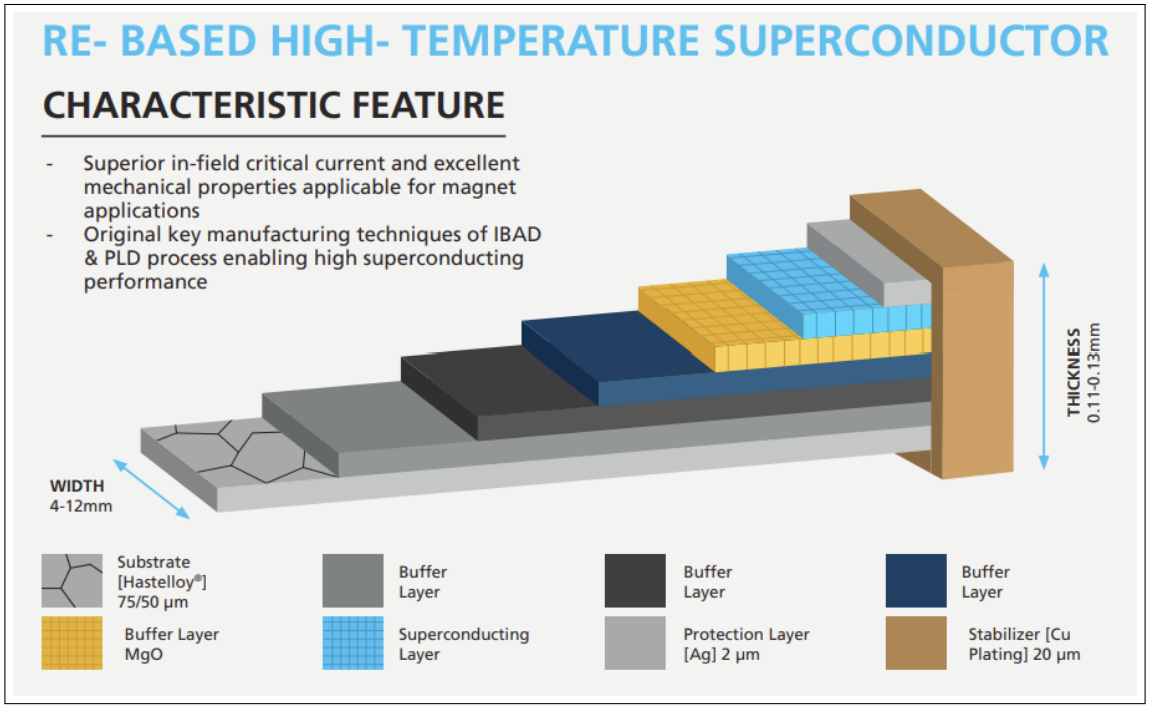

Figure 6.1: Fujikura tape layers [18]

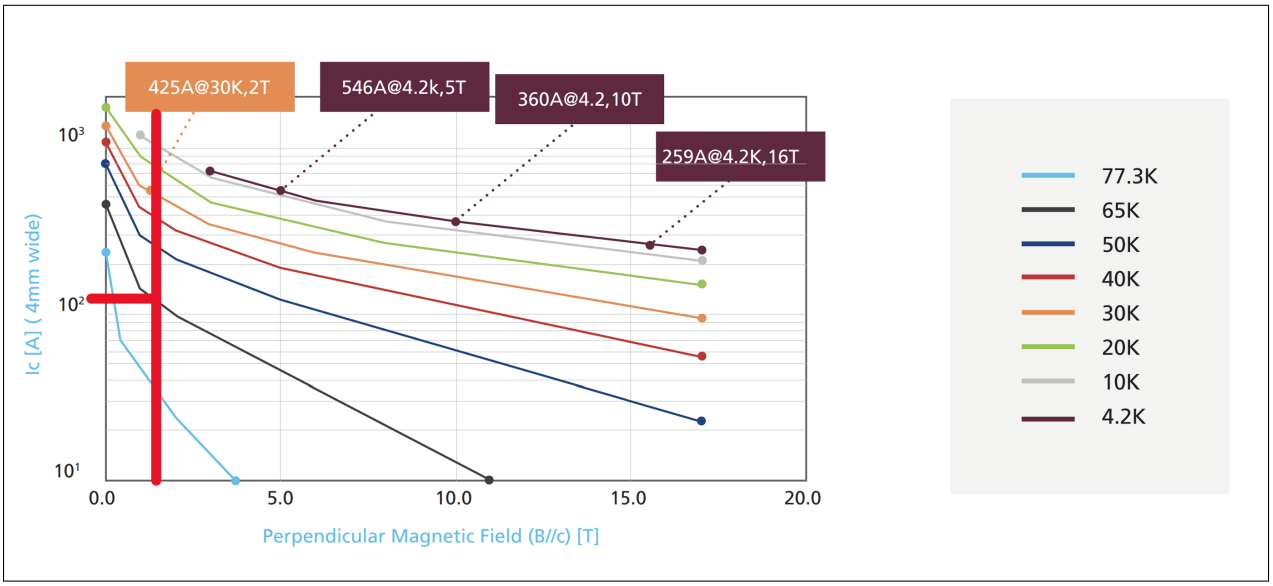

Figure 6.2: Critical current vs. magnetic field [18]

As shown in Figure 6.2, the desired magnetic field is 1.518 T. At 65 K, the critical current is 110 A. Due to possible temperature instabilities, the operating currents are less than the critical currents. Therefore, the operating currents were selected to be 100 A for a temperature of 65 K.

6.2 Coil and Iron Design

Coils were designed for two different cases: at 65 K with 3 pancakes and at 65 K with 4 pancakes. For both of these cases, the coil cross-sectional dimensions were determined, as shown in Table 5.2. These coils are made of REBCO tape. The temperature of 65 K was selected due to the tape's ability to conduct higher levels of current while maintaining a high critical temperature. With this temperature, the critical current value is 110 A. However, due to the possibility of temperature fluctuations during operation, a current of 100 A was used. This ensures that even in the case of a temperature fluctuation, the coil will remain in a superconducting state. The decision to use either 3 or 4 pancakes will be determined as this project progresses, once the power and winding implications have been explored. Following the methodology in Chapter 4, this led to 641 turns per coil and coil cross-sectional dimensions of 50 x 46 mm and 39 x 56 mm, for 3 and 4 pancakes, respectively. The overall shape of the coil was designed around the shape of the pole.

The iron was initially designed for the case of a resistive copper magnet. Using this case, the notch width and height for the iron were found by adding buffer space around the resistive coil geometry. The size of the notches for the resistive coils is significantly larger than the cross-sectional area of the superconducting coil. However, due to the vacuum chamber and thermal shield that surround the superconducting coil, the notch size for the superconducting magnet was not altered from the resistive case. The next aspect of the iron design was the pole (the two faces on either side of the pole gap, shown in Figure 5.3). The width of this component is defined by the desired region of field uniformity. The inner and outer curvature of this part is coradial with the central ion trajectory. After developing this part, the cross-sectional area was used to determine the areas of the yoke.

The iron, made of C1006 iron, is a high magnetic permeability component. As a result of this, the iron is able to absorb the excess magnetic field produced by the coils. The iron is designed such that within the pole gap, there is a uniform field of 1.5 T while the surrounding iron absorbs the remainder of the magnetic field.

6.3 Simulation

Magnetic field and force simulations were performed using Ansys Maxwell. The results of these simulations are discussed in this section.

6.3.1 Magnetic Field Simulation

The magnetic field simulation results are shown in Figures 5.5 and 5.6 for the 3 pancake and 4 pancake cases, respectively. The resulting contour plots for both cases are relatively similar. The maximum magnetic flux density is slightly different (2.4 T vs. 2.3 T), however, this maximum value is in a small, localized area.

In both plots, it can be seen that within the pole gap, the magnetic flux density is 1.33 T, slightly under the desired value of 1.5 T. Despite this value being lower than the desired magnetic flux density, within the pole gap, the field is uniform, varying by a maximum of roughly 0.005 T. This slight underperformance in magnetic flux density could be addressed by increasing the number of ampere-turns in the coil or increasing the current (also decreasing the temperature). Additionally, in both cases, it can be seen that there is no magnetic saturation in the iron. The slope of the B-H curve, shown in the Ansys material properties in Chapter 4, indicates the magnetic permeability of the material. Once the material reaches maximum magnetization, the slope of the curve flattens, meaning the material reaches the point of saturation. In this state, increasing the magnetic field strength (H) does not increase the magnetization of the material (B). Beyond the saturation point, the material essentially acts as free space and the magnetic field lines extend past the iron. In the simulations performed, since the iron does not become saturated, there are no stray field lines extending beyond the assembly. This indicates that the iron is sufficiently large to absorb the required magnetic field.

6.3.2 Magnetic Force Simulation

After performing magnetic field simulations, the magnetic force simulations were completed. The purpose of the force simulations is to provide insight into the structural requirements for supporting the coils. In both cases, the forces are relatively similar, with magnitudes of roughly 37 kN acting on each coil. The main component of this magnitude is in the vertical direction. However, there are minor forces acting in the x and z directions as well.

As a result of the relatively large force acting in the y direction, vertical supports will be required to support the coils. The supports used will be further explained when the preliminary cryogenic design is outlined.

6.4 Preliminary Cryogenic Design

This design shows a preliminary version of the cryogenic system that is to be used to cool the coils to superconducting temperatures. For thermal insulation purposes, a vacuum chamber surrounds the coil. The vacuum environment reduces any conductive or convective heat transfer that results from ambient conditions. The vacuum chamber is to have flanges for electrical feed-throughs and a vacuum connection. Within the vacuum chamber is a thermal shield layer. This layer is internally connected to the vacuum chamber. The cryocooler stage is thermally connected to this layer. Within the thermal shield is the coil. The coil is suspended from the strongback part of the thermal shield layer. The coil is wrapped in a layer of insulation.

Structural supports are required to constrain each of the layers surrounding the coil. These structural supports are to be designed to minimize conductive heat transfer between components. As a result of the magnetic force simulations, it was determined that the majority of the magnetic force is in the vertical direction. Therefore, these thermally isolating supports should be primarily constraining vertical movement.

In Figure 5.8, the cryocoolers are positioned within the pole gap. This configuration was selected as it didn't take away any material from the iron. Removing iron material would increase the magnetic flux density in other regions. However, based on preliminary dimensions, the ability to fit a cryocooler within the pole gap depends on the cryocooler selected. In the event that the cryocooler does not fit within the pole gap, the notch width could be increased and the cryocoolers could be added in a horizontal configuration, as shown in Figure 6.3.

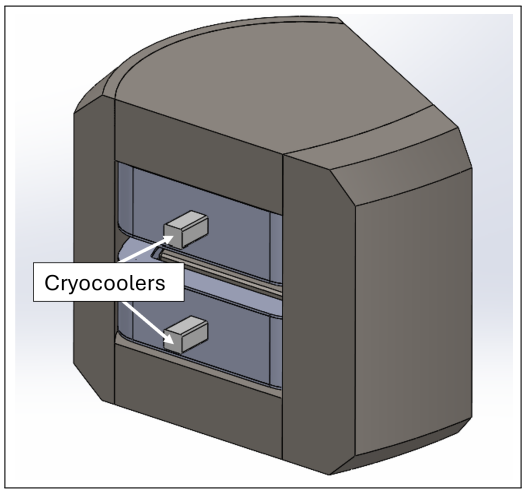

Figure 6.3: Alternative cryocooler configuration

6.5 Summary

This chapter discusses the results of this project. First, a deeper look into the material selection criteria is conducted. The primary selection criteria for each material was material availability, critical temperature, critical current, and cost. The reasoning behind the weight factors and the strengths and weaknesses of each material are also discussed. Next, the iron and coil design process is discussed, including design decisions. The next section discusses the results of the magnetic field and force simulations. The field simulations revealed a uniform magnetic field of 1.33 T within the pole gap. Additionally, it was shown that no magnetic saturation occurs within the iron. The force simulations showed a force of approximately 37 kN acting on each coil (in opposing directions). Finally, the preliminary cryogenic design was discussed, including the requirement for certain components, and the positioning of the cryocoolers.

Chapter 7

Conclusion and Future Work

This project has met the objectives of material selection, design and simulation by following the explained methodologies. However, there are still areas to be pursued and researched in the future.

7.1 Conclusion

The goal of this project was to design a superconducting coil to be used in a mass spectrometer. This coil would be used to replace the resistive copper coil that is currently used to deflect the ions in D-Pace's mass spectrometer. This project is motivated by the challenges associated with resistive coils, including their power consumption, size, and field instabilities. Superconductors are capable of conducting current without losses to resistance. This allows for less power consumption, higher magnetic fields (smaller assemblies), and constant current (no field instability). The objectives of this project were to select a superconducting material to be used for the coils, to design and model the coil and surrounding iron, to simulate the magnetic field and the magnetic force, and to establish a preliminary design of the cryogenic system.

After evaluating NbTi, REBCO, and BSCCO, REBCO was the material selected to be used for the superconducting coils. The production of REBCO is increasing as research into this material increases. However, the material is currently produced by several companies including SuperPower, Fujikura, Sumitomo, and Bruker. Additionally, the cost of the raw materials is relatively low. Finally, the critical parameters of REBCO are very promising as it has a maximum critical temperature of 92 K and a critical current density of 10^7, one of the highest current densities available.

Next, the coil was designed to operate at 100 A and 65 K. Using these values, two cross-sections were determined, one using 3 pancakes, the other 4 pancakes. The decision to use either 3 or 4 pancakes will be determined at a later date when the power and winding implications have been explored. After determining the coil cross-section, the iron was designed. With the desired area of field uniformity, the pole geometry was determined. The coil shape is based on this. The rest of the iron was designed based on taking a ratio between the pole area and the yoke area in order to adequately distribute the field between the pole and iron. The 1.5 T magnetic field resulting from the coils produces a uniform field within the pole gap of the mass spectrometer. The iron is designed to absorb the excess magnetic field resulting from the coils without becoming saturated.

After completing the design of the coil and iron, the designs were validated using Ansys simulations. The magnetic field simulation results show contour plots with the magnetic flux density at varying points in the assembly. The simulations showed a uniform magnetic field of 1.33 T within the pole gap. Additionally, it revealed that the iron adequately absorbs the excess magnetic field lines without becoming saturated. The magnetic force simulations revealed forces of approximately 37 kN acting vertically on each of the coils in opposite directions.

The final objective to complete in this project was to establish a preliminary cryogenic design. In order to bring the coils to a superconducting state, they need to be cooled to cryogenic temperatures. In order to thermally isolate the coil from convective and conductive heat transfer sources, it is put within a vacuum chamber. Additionally, within the vacuum chamber, a thermal shield and insulation surround the coil. To extract the heat, a cryocooler is used. Due to the size of this component, the positioning will be determined once a cryocooler has been selected.

7.2 Future Work

As this project of replacing the copper resistive magnet with a superconducting magnet continues to be developed, there are a number of areas for future work. The main areas include furthering the cryogenic design, designing the structural support system for supporting the vacuum chamber, thermal shield, and coil, and the design of the current lead system.

In order to further the cryogenic design, a full thermal analysis needs to be completed. This will include identifying the heat transfer loads coming from the external environment. Additionally, materials for different components need to be selected in order to quantify the

heat transfer resulting from these components. After completing this analysis, a cryocooler can be selected based on the heat that needs to be extracted from the system. Based on the cryocooler selected, the power consumption required for this system can be compared in a quantifiable manner to the power consumption resulting from the resistive coil system.

A full structural analysis and design also needs to be undertaken for this system. The loading presented from Ansys magnetic force simulations is a starting point for this process however, additional forces, including gravity and thermal forces, need to be considered for future analysis. Once the forces acting on the system are adequately quantified, the support structures can be designed. Through this design process, the thermal impact of the supports needs to be considered to avoid conductive heat transfer through the supports. Materials with low thermal conductivity should be used.

Another aspect of this project to be considered in the future is the current lead design. This system should be designed to deliver current to the coils while minimizing the production of heat.

7.3 Summary

This chapter concludes the project, starting with the outcomes of the work completed and finishing with the work that is still to be completed moving forward. The objectives of this project were met, including the selection of a material, the design and modeling of the coil and iron, the simulation of the magnetic flux density and magnetic force, and finally, the preliminary design of the cryogenic system. Moving forward, there is still a significant amount of work to be completed. A detailed cryogenic design needs to be completed, requiring a full thermal analysis in order to properly spec a cryocooler. Additionally, a full structural analysis and design need to take place. Lastly, a current lead design needs to be completed to reduce the amount of heat being brought into the system as the current is being delivered.

Bibliography

[1] J. Clark, "How the mass spectrometer works," LibreTexts Chemistry.

[2] S. R. Thomas, J. L. Ackerman, and J. H. Kereiakes, "Practical aspects involved in the design and set up of a 0.15 T, 6-coil resistive magnet, whole body nmr imaging facility," *Magnetic Resonance Imaging*, 1984.

[3] R. Wengenmayr, "Superconductivity is pair work," Max Planck Research, 2011.

[4] J. Weisend, *Handbook of Cryogenic Engineering*. Taylor Francis, 1998.

[5] M. Ladd, H. Quick, O. Speck, M. Bock, A. Doerfler, M. Forsting, J. Hennig, and B. Ittermann, "Germany's journey toward 14 tesla human magnetic resonance," *Magnetic Resonance Materials in Physics, Biology and Medicine*, 2023.

[6] "Pinning: Superconductivity's footprint," Universite Paris Saclay, https://hebergement.universite-paris-saclay.fr/supraconductivite/supra/en/supra-levitation-piegage-more.php.

[7] M. Parizh, Y. Lvovsky, and M. Sumption, "Conductors for commercial MRI magnets beyond NbTi: requirements and challenges," *Superconductor Science and Technology*, 2016.

[8] "Superconducting magnets," Questions and Answers in MRI, https://mriquestions.com/superconductive-design.html.

[9] "ITER magnets," https://www.iter.org/mach/Magnets.

[10] C. Yao and Y. Ma, "Superconducting materials: Challenges and opportunities for large-scale applications," *iScience*, 2011.

[11] C. Barth, "High temperature superconductor cable concepts for fusion magnets," Ph.D. dissertation, Karlsruhe Institute of Technology, 2013.

[12] M. P. abd Venkat Selvamanickam, "Development of RE-Ba-Cu-O superconductors in the U.S. for ultra high field magnets," *Superconducting Science and Technology*, 2022.

[13] "2g hts wire specification," SuperPower, https://www.superpower-inc.com/specification.aspx.

[14] H. Reiss, "The additive approximation for heat transfer and for stability calculations in a multi-filamentary superconductor - part a," *Journal of Superconductivity and Novel Magnetism*, vol. 32, 11 2019.

[15] R. Slade, M. J. Mallett, and V. Chamritski, "Development of a cryogen free 1.5 T YBCO HTS magnet for MRI," *IEEE Transactions on Applied Superconductivity*, 2013.

[16] D. Larbalestier, H. Weijers, J. Jaroszynski, and A. Xu, "Design of a superconducting 32 T magnet with REBCO high field coils," *IEEE Transactions on Applied Superconductivity*, 2012.

[17] B. Parkinson, K. Bouloukakis, and R. Slade, "A compact 3 t all hts cryogen-free mri system," *Superconductor Science and Technology*, 2017.

[18] "Fujikura Superconductor Guide," Fujikura, https://www.fujikura.co.uk/netalogue/pdfs/Fujikura

Appendix A

Coil Geometry

A.1 MATLAB Coil Dimensions Function

The following MATLAB function is used to determine the number of turns per coil, the coil width, and the coil height by inputting the desired temperature and number of pancakes.

```
function [coil_w, coil_h, n] = coil_dims(pancakes, temp)
   %particle momentum p [MeV/c]
   p=140.26;

   %central trajectory radius rho [mm]
   rho=309.3972;

   %magnetic flux density B [T]
   B=1.518;

   %trial ampere turns NI [Amp-turns]
   NI=64023;

   %critical current Ic [A]
   if temp==50
       Ic=230;
   elseif temp==65
       Ic=100;
   end
```

```
    %turns per coil
    n = NI/Ic;
    n=ceil(n);

    %tape dimensions [mm]
    thickness = 0.13;
    height = 4;

    %current density J [A/mm^2]
    J = Ic/(thickness*height);

    %number of turns per pancake
    tp=ceil(n/pancakes);

    %coil width [mm]
    coil_w=ceil((tp*thickness)+((tp+1)*0.076)+(2*0.52)+(2*2));

    %coil height [mm]
    coil_h=ceil(pancakes*height+(pancakes+1)*6.35+8*0.52+2*2);
end
```

A.2 Coil Geometry Calculations

The following calculations determine the geometry of a resistive copper coil with 4 pancakes.

Using a maximum current of 190.5 A, the number of turns per coil can be determined:

$$N_{turns} = \frac{64023 \text{ Amp Turns per Pole}}{190.5\,\text{A}} = 336 \text{ Turns per coil}$$

With an operating current of 190.5 A, the current density in the magnet is:

$$J_{max} = \frac{190.5\,\text{A}}{(63.1\,\text{mm})(1.246\,\text{mm})} = 2.42\,\text{A/mm}^2$$

At this point, the coil width is determined to be 117 mm.

$$\text{Coil width= (Copper tape) + (Mylar) + (Pancake wrap) + (Coil over-wrap)}$$

$$\text{Coil width} = 84(1.246\,\text{mm}) + 85(0.076\,\text{mm}) + 2(0.52\,\text{mm}) + 2(2\,\text{mm}) = 116.16\,\text{mm}$$

Next, the coil height is determined to be 297 mm.

$$\text{Coil height= (Mylar) + (Cooling plate) + (Pancake wrap) + (Coil over-wrap)}$$

$$\text{Coil height} = 4(64.1\,\text{mm}) + 5(6.35\,\text{mm}) + 8(0.52\,\text{mm}) + 2(2\,\text{mm}) = 296.31\,\text{mm}$$

The coil cross section is shown in Figure A.1 below. This includes a structure of 4 pancakes, each of 84 turns with copper tape.

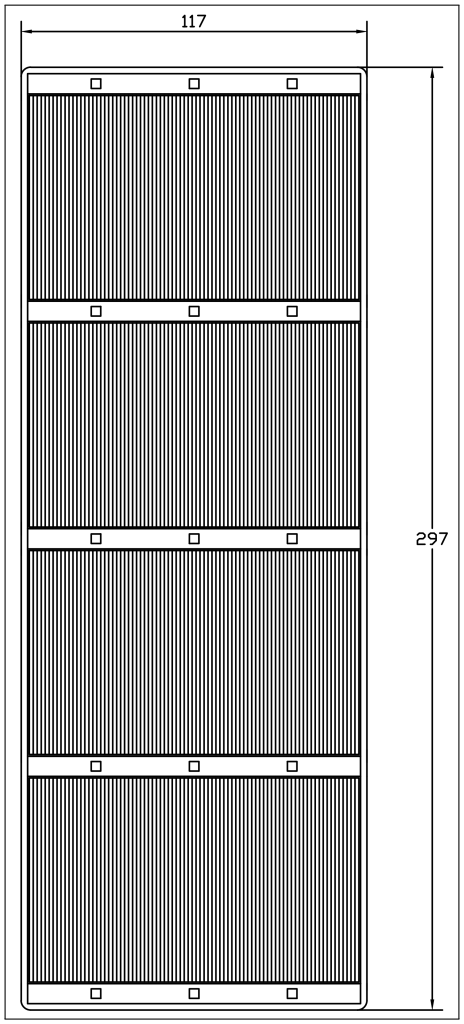

Figure A.1: Coil cross section (dimensions in millimeters)

Appendix B

Iron Geometry

As a result of the rule of thumb that the pole width is a factor of 5 times as large as the good field region of ±44 mm for the desired level of uniformity for a 100 mm gap, the pole width w is equal to:

$$w = (5)(44) = 440\,\text{mm}$$

The coil notch in the yoke is chosen to be coil width plus 5 mm buffer space on either side of the coil. The notch height for the coil (up to the top of the pole chamfer of 10 mm) is coil height plus 3 mm to include space for neoprene underneath the coil.

Using the previously defined coil width and height of 117 mm and 297 mm, the notch width and height are determined:

$$\text{Coil notch width} = 117\,\text{mm} + (2)(5\,\text{mm}) = 127\,\text{mm}$$

$$\text{Coil notch height} = 297\,\text{mm} + 3\,\text{mm} = 300\,\text{mm}$$

Next, the pole and yoke areas are determined. As defined above, the radius of curvature of the central trajectory is 309.3972 mm. Additionally, the pole width was determined to be 440 mm.

The partial pole (P1) width is therefore half of this, 220 mm. The outer radius of P1 is therefore 309.3972 mm + 220 mm = 529.3972 mm.

The partial pole (P2) width is also 220 mm. The outer radius of P2 is the central trajectory.

The inner radius of P2 is therefore 309.3972 mm - 220 mm = 89.3972 mm.

Using Solidworks, the area of P1 was determined to be 153 242.5049 mm^2 and the area of P2 was determined to be 150 586.5385 mm^2.

With this information, the yoke areas are found. It is desired to have a larger field in the poles than in the yokes. Therefore, the yoke areas are to be larger than the pole areas by a factor of 1.5/1.2.

Yoke 1:

$$(1.2)A_{Y1} = (1.5)A_{P1}$$

$$A_{Y1} = \frac{1.5}{1.2}(A_{P1}) = \frac{1.5}{1.2}(153\,242.5049\,\text{mm}^2) = 191\,553.131\,\text{mm}^2$$

Yoke 2:

$$(1.2)A_{Y2} = (1.5)A_{P2}$$

$$A_{Y2} = \frac{1.5}{1.2}(A_{P2}) = \frac{1.5}{1.2}(150\,586.5385\,\text{mm}^2) = 188\,233.173\,\text{mm}^2$$

The plan view showing the cross-sectional areas of the poles and yokes is shown in Figure B.1 below.

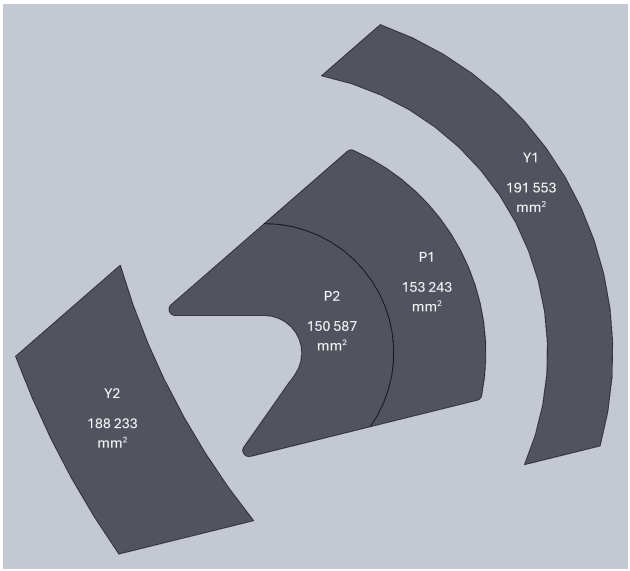

Figure B.1: Pole and yoke areas

The dimensioned cross-sectional view of the resistive coil assembly (including the coil, poles

and yokes) is shown in Figure B.2 below.

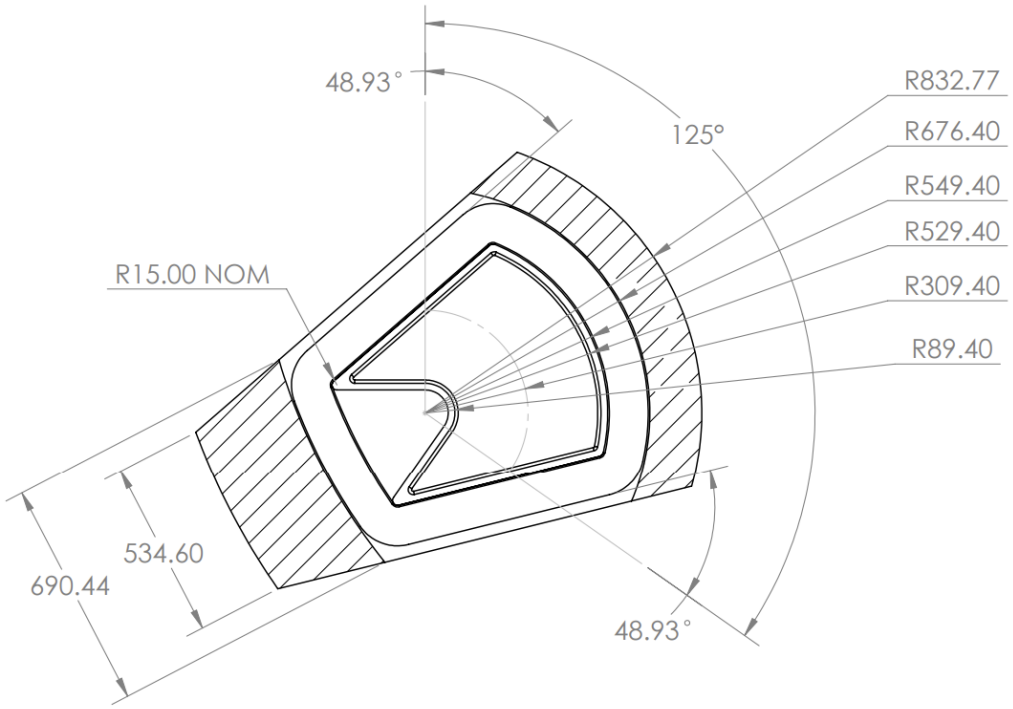

Figure B.2: Plan view cross section

Appendix C

Resistive Coil Power

The following calculations go through an example of calculating the power consumption of a resistive coil.

From the Solidworks model of the resistive coil, the median turn length is equal to 2883.01 mm.

Therefore, the total conductor length per coil is equal to:

$$\text{Total conductor length per coil} = (336\,\text{turns})(288.3\,\text{cm/turn}) = 96\,868.97\,\text{cm}$$

Next, at a temperature of 20°C, the resistance can be determined.

$$R_{20^o} = \rho_{Cu}\frac{\text{Total Conductor Length}}{\text{Conductor Cross-Sectional Area}}$$

$$R_{20^o} = (1.673 \times 10^{-6}\ \Omega\ \text{cm})\frac{(96\,868.97\,\text{cm})}{(6.31\,\text{cm})(0.1246\,\text{cm})} = 0.206\ \Omega\ \text{per coil}$$

Using this value and the assumption that the maximum ΔT is 40°, the resistance R_{hot} is calculated.

$$R_{hot} = R_{20^\circ}[1 + (\Delta T)(\text{Temperature Coefficient of Copper})]$$

$$R_{hot} = (0.206\,\Omega)[1 + (40^\circ)(0.003\,93\,\Omega/^\circ\text{C})] = 0.239\,\Omega$$

With this value, along with the current (190.5 A), the voltage drop per coil is found.

$$V_{coil} = (I_{max})(R_{hot}) = (190.5\,\mathrm{A})(0.239\,\Omega) = 45.44\,\mathrm{V}$$

Therefore, the voltage for the entire magnet (2 coils) is:

$$V_{magnet} = (2)(45.44\,\mathrm{V}) = 90.88\,\mathrm{V}$$

Finally, the power requirement is determined:

$$P = V_{magnet} I_{max} = (90.88\,\mathrm{V})(190.5\,\mathrm{A}) = 17\,312.57\,\mathrm{W}$$

Appendix D

Preliminary Drawings

Appendix D includes preliminary drawings of the designs. The drawings included are:

- Iron and coil assembly
- REBCO coil - 3 pancakes, 65 K
- REBCO coil - 4 pancakes, 65 K

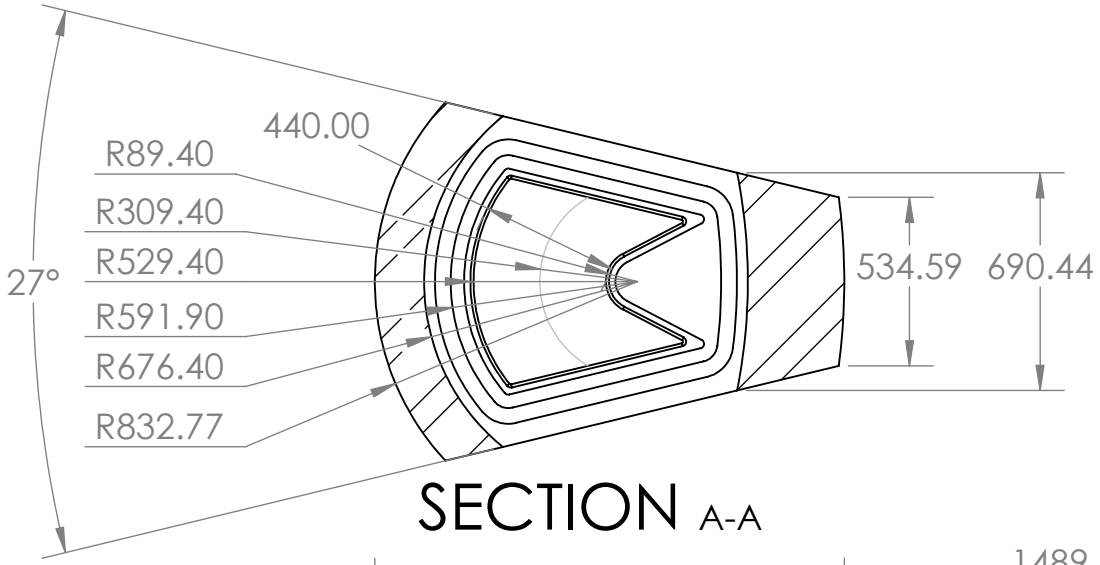

SECTION A-A

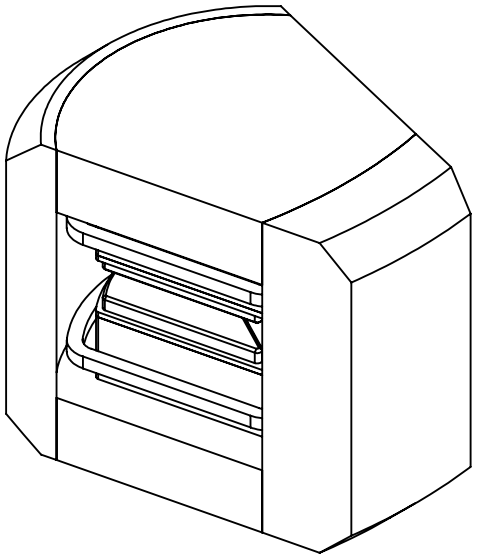

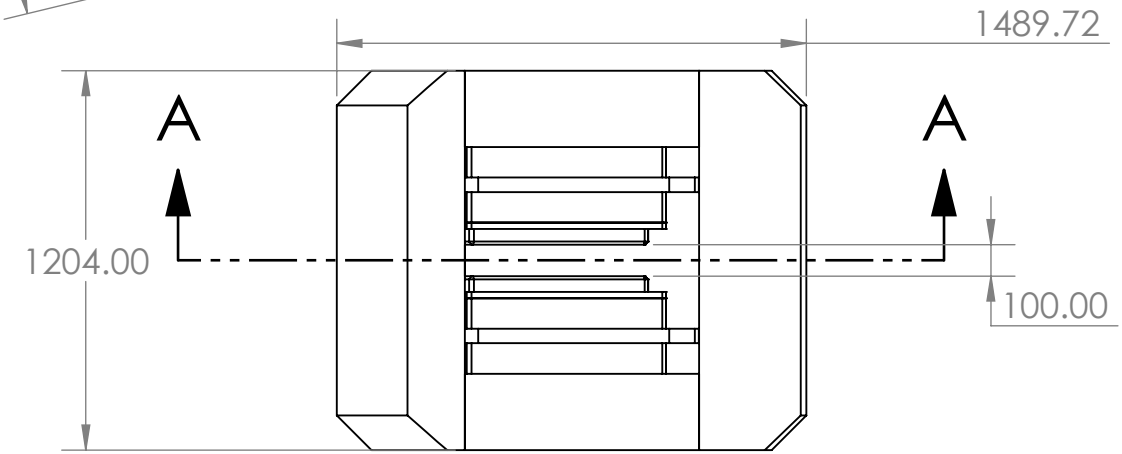

		UNLESS OTHERWISE SPECIFIED:		NAME	DATE
		DIMENSIONS ARE IN MILLIMETERS TOLERANCES: FRACTIONAL ± ANGULAR: MACH ± BEND ± TWO PLACE DECIMAL ± THREE PLACE DECIMAL ±	DRAWN	ID	
			CHECKED		
			ENG APPR.		
			MFG APPR.		
		INTERPRET GEOMETRIC TOLERANCING PER:	Q.A.		
		MATERIAL	COMMENTS:		
NEXT ASSY	USED ON	FINISH			
APPLICATION		DO NOT SCALE DRAWING			

TITLE:

ASSEMBLY (3 PAN. COIL)

SIZE	DWG. NO.	REV
A		
SCALE: 1:24	WEIGHT:	SHEET 1 OF 1

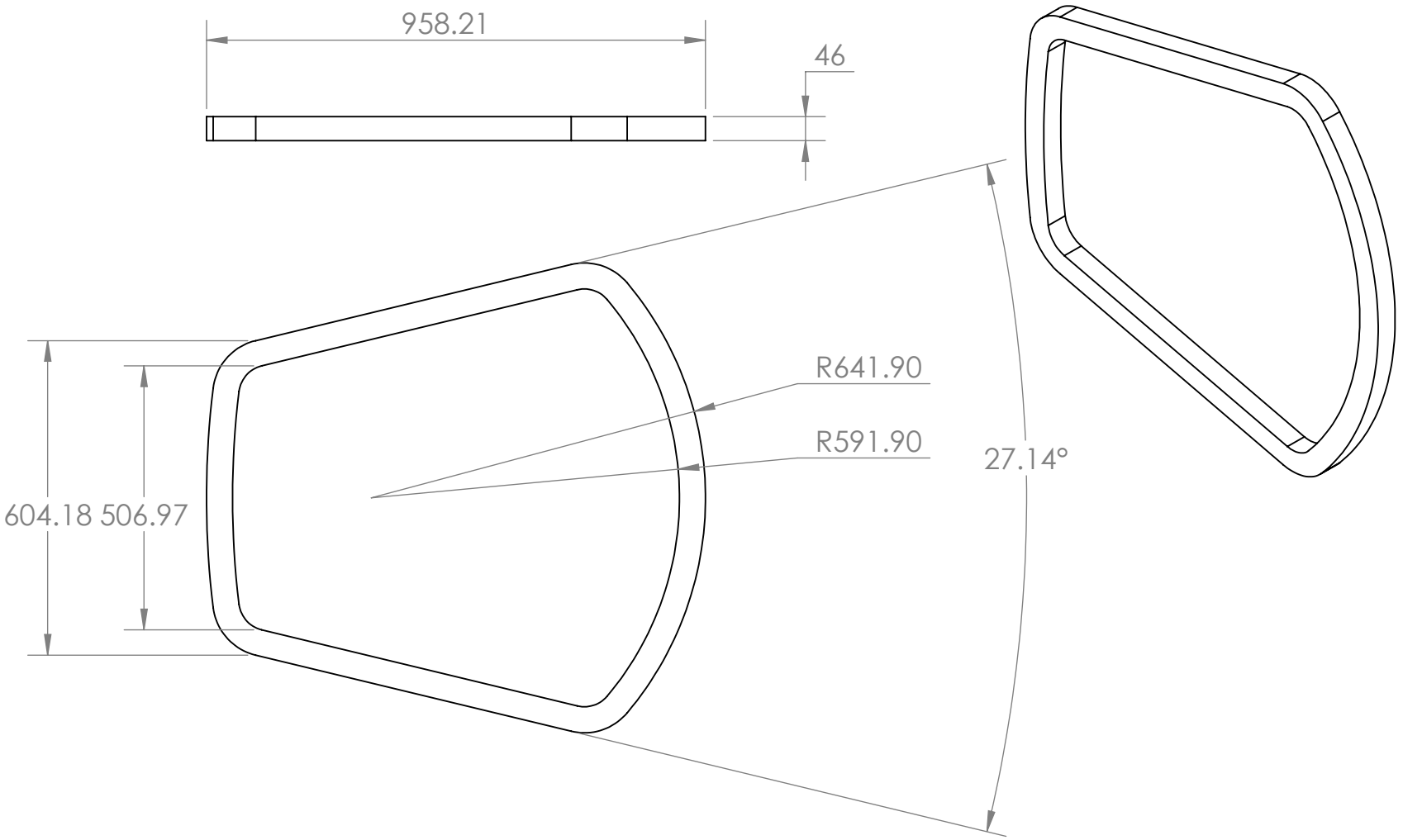

		UNLESS OTHERWISE SPECIFIED:		NAME	DATE
		DIMENSIONS ARE IN MILLIMETERS TOLERANCES: FRACTIONAL ± ANGULAR: MACH ± BEND ± TWO PLACE DECIMAL ± THREE PLACE DECIMAL ±	DRAWN	ID	
			CHECKED		
			ENG APPR.		
			MFG APPR.		
		INTERPRET GEOMETRIC TOLERANCING PER:	Q.A.		
		MATERIAL	COMMENTS:		
NEXT ASSY	USED ON	FINISH			
APPLICATION		DO NOT SCALE DRAWING			

TITLE:

REBCO COIL 3 PAN. 65 K

SIZE	DWG. NO.	REV
A		

SCALE: 1:12 | WEIGHT: | SHEET 1 OF 1

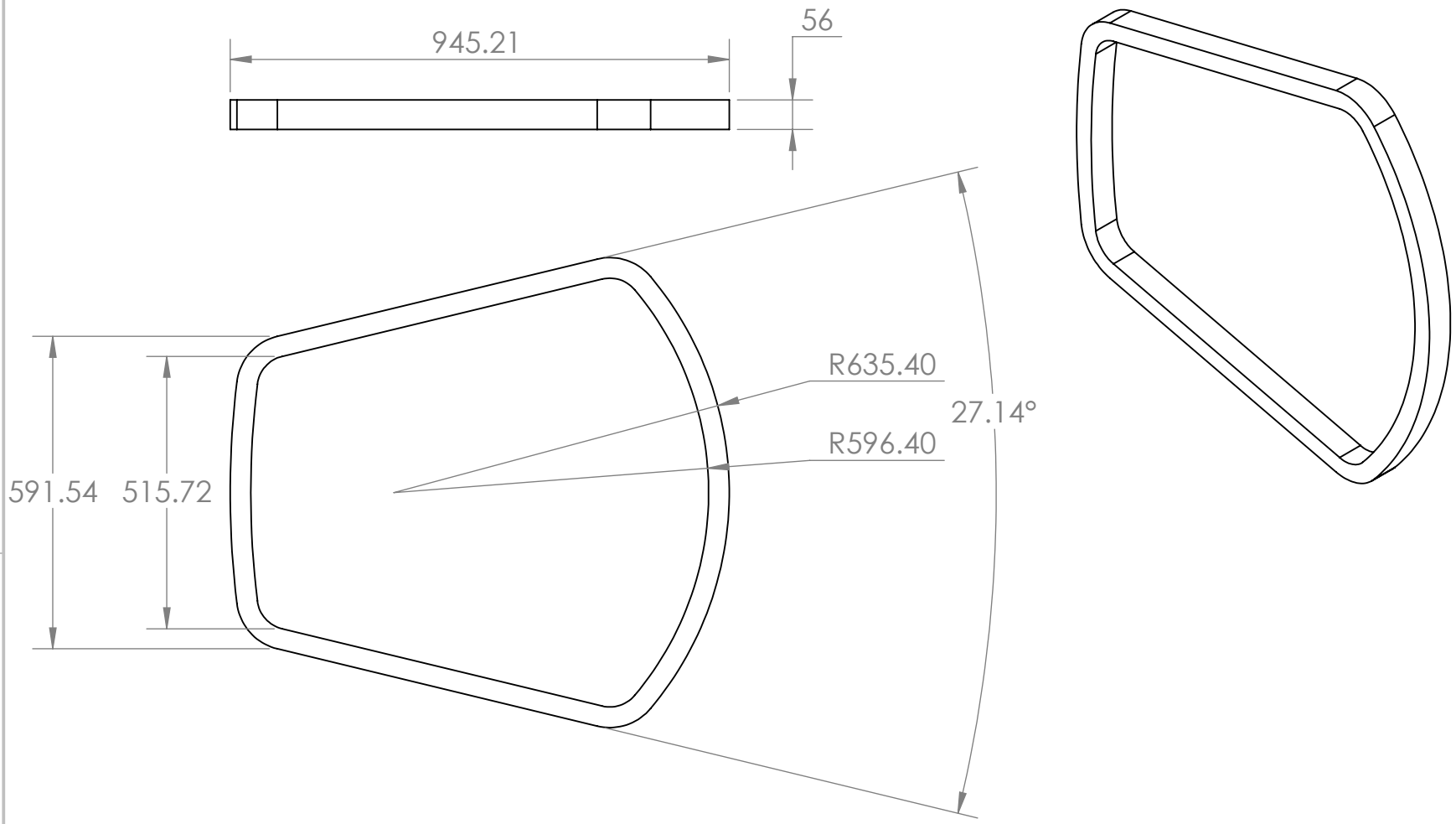

		UNLESS OTHERWISE SPECIFIED:		NAME	DATE
		DIMENSIONS ARE IN MILLIMETERS TOLERANCES: FRACTIONAL ± ANGULAR: MACH ± BEND ± TWO PLACE DECIMAL ± THREE PLACE DECIMAL ±	DRAWN	ID	
			CHECKED		
			ENG APPR.		
			MFG APPR.		
		INTERPRET GEOMETRIC TOLERANCING PER:	Q.A.		
		MATERIAL	COMMENTS:		
NEXT ASSY	USED ON	FINISH			
APPLICATION		DO NOT SCALE DRAWING			

TITLE:

REBCO COIL 4 PAN. 65 K

SIZE	DWG. NO.	REV
A		

SCALE: 1:12	WEIGHT:	SHEET 1 OF 1